Tissue and Cell xxx (xxxx) 102701

Contents lists available at ScienceDirect

Tissue and Cell

journal homepage: www.elsevier.com/locate/tice

# Structural isomers of carene persuade apoptotic cell death by inhibiting cell cycle in breast cancer cells: An *in silico* and *in vitro* approach

Haribalan Perumalsamy [a, b, 1, *], Johan Sukweenadhi [c], Anuj Ranjan [d], Akhilesh Dubey [e], Manohar Mahadev [e], Mohamed Farouk Elsadek [f], Saeedah Musaed Almutairi [g], Daewon Sohn [b, h], Sri Renukadevi Balusamy [i, 1, **]

[a] *Center for Creative Convergence Education, Hanyang University, Seoul 04763, Republic of Korea*
[b] *Research Institute for Convergence of Basic Science, Hanyang University, Seoul 04763, Republic of Korea*
[c] *Faculty of Biotechnology, University of Surabaya, Surabaya 60293, Indonesia*
[d] *Academy of Biology and Biotechnology, Southern Federal University, Rostov-on-Don 344006, Russia*
[e] *Department of Pharmaceutics, NGSM Institute of Pharmaceutical Sciences, NITTE (Deemed to be University), Mangaluru, India*
[f] *Department of Biochemistry, College of Science, King Saud University, P.O. 2455, Riyadh 11451, Saudi Arabia*
[g] *Department of Botany and Microbiology, College of Science, King Saud University, P.O. 2455, Riyadh 11451, Saudi Arabia*
[h] *Department of Chemistry, College of Natural Sciences, Hanyang University, Seoul 04763, Republic of Korea*
[i] *Department of Food Science and Biotechnology, Sejong University, Gwangjin-gu, Seoul, Republic of Korea*

ARTICLE INFO

*Keywords:*
Carene isoforms
Apoptosis
Cell cycle
*Piper nigrum*
Hydro distillation

ABSTRACT

For the first time, our study provides a comprehensive examination of the anti-cancer effects of structural isomers of carene in breast cancer cells, specifically focusing on cell cycle inhibition and the induction of apoptosis. We utilized the hydro-distillation method to extract *Piper nigrum* seed essential oil (PNS-EO) and identified its bioactive components through gas chromatography-mass spectrometry (GC-MS) analysis. A total of 46 bioactive compounds were isolated via hydro-distillation, identified through GC-MS analysis, and validated by co-injection using GC analysis. The major constituent, 3-carene displayed the most substantial anti-proliferative effect on the breast cancer cell line MCF-7, with an $IC_{50}$ value of 11.19 μg/mL. Further, docking studies were conducted to evaluate the putative role of 3-carene in inhibiting the cell cycle proteins (CDKN2A, CCND1, CDK4), as well as proteins in the apoptosis pathway (BCL-XL, BAX, BAK, Caspase 3). Additionally, we employed fluorescence-activated cell sorting (FACS) and clonogenic assays to evaluate cell cycle inhibition and time-dependent initiation of apoptosis. Moreover, fluorescence techniques including Terminal deoxynucleotidyl transferase dUTP nick end labeling (TUNEL), Hoechst staining, and Propidium iodide (PI) staining were performed to assess cell death and apoptosis. Furthermore, molecular techniques such as quantitative real-time PCR (qPCR) and western blotting were utilized to investigate the mechanism of cell death was elucidated through the inhibition of BCL2, MMP2, MMP9, and AKT expression, alongside the activation of BAX, cytochrome C, and Caspases 3 and 9. Our findings indicate that 3-carene, isolated through hydro-distillation, effectively hinders the cell cycle and promotes apoptosis in MCF-7 cells. Consequently, it shows promise for incorporation into combinational anti-cancer therapies, warranting further research.

*Abbreviations:* PNS-EO, *Piper nigrum* seed essential oil; GC-MS, Gas-chromatography-mass spectrum; QPCR, quantitative real-time PCR; FACS, Fluorescence-activated cell sorting; TUNEL,, Terminal deoxynucleotidyl transferase dUTP nick end labeling; PI, Propidium iodide; RPMI, Rosewell Park Memorial Institute; FBS, Fetal bovine serum,; EDTA, Trypsin-ethylenediaminetetraacetic acid; ATCC, American Type Culture Collection; FID, Flame ionization detector; MRC-5, human fetal lung fibroblast cell line; MCF-7, breast cancer lines

* Correspondence to: Creative Convergence Education, Department of Chemistry, Hanyang University, Seoul 04763, Korea
** Corresponding author.
*E-mail addresses:* harijai2004@gmail.com (H. Perumalsamy), renubalu@sejong.ac.kr (S.R. Balusamy).
[1] Equally contributed as first author.

https://doi.org/10.1016/j.tice.2024.102701
Received 20 September 2024; Received in revised form 17 December 2024; Accepted 18 December 2024

## 1. Introduction

The exploration of natural plant-based products for therapeutic applications has garnered significant attention in recent years. Our study focuses on isolating essential oil from *Piper nigrum* seed, known globally as black pepper. *Piper nigrum* is a perennial climbing vine widely distributed in tropical regions, with significant cultivation in India, Indonesia, Vietnam, and Brazil. The geographic distribution of *Piper nigrum* profoundly influences the concentration and composition of its bioactive components due to variations in climate, soil, and cultivation practices, emphasizing the importance of studying region-specific plants to achieve the highest bioactive yield (Li et al., 2020; Sen et al., 2016; Takooree et al., 2019). Bioactive compounds in *Piper nigrum*, such as piperine, exhibit diverse biological activities including antioxidant, anti-inflammatory, and anticancer properties (Duan et al., 2022; Turrini et al., 2020). The concentration of piperine and other secondary metabolites can significantly vary among different species and cultivars of *Piper nigrum*. For instance, studies have shown that *Piper nigrum* from different growing regions can exhibit distinct profiles of monoterpenes and sesquiterpenes, key constituents contributing to its therapeutic potential (Al-Khayri et al., 2022; Jaidee et al., 2022; Yu et al., 2022). Therefore, studying plants that are grown in specific regions is extremely important to select *Piper nigrum* as potential therapeutics. Despite the promising biological activities demonstrated by *Piper nigrum*, there is still a lack of comprehensive studies involved in understanding complex bioactive compound's anticancer potential. Further research is essential to fully elucidate the mechanisms of action and therapeutic efficacy of its essential oil derived compounds.

Carene, a naturally occurring bicyclic monoterpene found in essential oils from various plants such as rosemary, pine, and cedar, has garnered attention for its potential anticancer properties. This compound is particularly intriguing due to its dual active groups: a carbon-carbon double bond and a gem-dimethyl cyclopropane ring. This feature confers to its broad spectrum of activities like antimicrobial (Shu et al., 2019), antioxidant (Clarke, 2008), sedative (Woo et al., 2019), anti-inflammatory properties (Basholli-Salihu et al., 2017) and antifungal properties (Kang et al., 2019). While its anticancer potential has not yet been fully explored, articles have predicted that the molecule might exhibit anticancer properties (Kang et al., 2019). To the best of our knowledge, this is the first report on the 3-carene from *Piper nigrum* seed essential oil (PNS-EO) which induced apoptosis by arresting cell cycle and metastasis.

**Table 1**
Primers were used for real-time quantitative reverse transcription polymerase chain reaction in this study.

| Gene | RefSeq ID | Forward primer and Reverse primer | cDNA amplicon size |
|---|---|---|---|
| *Bax* | NM_004324.3 | 5′-TTCTGACGGCAACTTCAACTG−3′<br>5′-GTTCTGATCAGTTCCGGCA−3′ | 104 |
| *Bcl−2* | NM_000657 | 5'-AGCACTCCCGCCACAAAGA−3'<br>5'-ATCCAGGTGTGCAGGTG−3' | 133 |
| *Akt−1* | NM_005163.2 | 5′-CAAGCCCAAGCACCGC−3′<br>5′-GGATCACCTTGCCGAAAGTG−3′ | 67 |
| *MMP−2* | NM_001127891.1 | 5'-AGTCTGAAGAGCGTGAAG −3'<br>5'-CCAGGTAGGAGTGAGAAT G−3' | 174 |
| *MMP−9* | NM_004994.2 | 5'-TGACAGCGACAAGAAGTG−3'<br>5'-CAGTGAAGCGGTACATAGG−3' | 175 |
| *CAS−8* | NM_001228 | 5'-GAAAAGCAAACCTCGGGGATAC−3'<br>5'-CCAAGTGTGTTCCATTCCTGTC−3' | 111 |
| *CAS−9* | NM_001229 | 5'-CCAGAGATTGCGAAACCAGAGG−3'<br>5'-GAGCACCGACATCACCAAATCC−3' | 87 |
| *β-actin* | NM_001101.3 | 5′-CGGGAAATCGTGCGTGAC−3′<br>5'-AGCTCTTCTCCAGGGAGGA−3' | 102 |

Breast cancer remains a leading cause of morbidity and mortality among women worldwide, necessitating the development of novel and effective therapeutic strategies. In recent years, many anticancer treatments have been associated with high toxicity levels and the development of drug resistance. The promising and effective strategy is to identify drugs that can induce apoptosis by inhibiting tumor growth and metastasis in cancer cell lines.

Apoptosis, or programmed cell death, is hence, a crucial mechanism by which cancer cells can be selectively targeted and eliminated without affecting normal cells (Pfeffer and Singh, 2018). The induction of apoptosis in cancer cells is a key objective in cancer therapy, making compounds that can trigger this process highly valuable (Carneiro and El-Deiry, 2020). Pro-apoptotic compounds, hence, sourced from either synthetic chemistry or natural origins, provide an alternative due to their therapeutic effects and targeted action on cancer cells, while having minimal or no adverse effects on normal mammalian cells (Perumalsamy et al., 2017). The underlying mechanisms through which 3-carene exerts its anticancer effects involve modulation of various cellular pathways, including those governing cell cycle regulation, oxidative stress response, and apoptotic signaling is crucial for effective anticancer treatment.

We aim to isolate 3-carene from PNS-EO using the hydro-distillation method to systematically understand the mechanisms underlying 3-carene's anti-cancer potential both *in silico* and *in vitro* that benefit complementary practice. Continued research into its mechanisms and therapeutic applications *in vivo* could lead to the use of 3-carene in breast cancer therapy.

## 2. Materials and methods

### 2.1. Materials

*Piper nigrum* seeds were purchased in an Oriental medicinal store in Jongno District, Seoul, South Korea. The commercially available high-grade compounds were purchased from Sigma-Aldrich (St. Louis, MO, USA) and used as standard. The cell culture medium and reagents such as Rosewell Park Memorial Institute (RPMI 1640), fetal bovine serum (FBS), antibiotic-antimycotic solution, trypsin-ethylenediaminetetraacetic acid (EDTA (0.5 %)) was purchased from Gibco (Life Technologies NY, USA). For fluorescence staining analysis, Hoechst 33258, PI, and RNase were bought from Sigma-Aldrich (St. Louis, MO, USA). Thermo Scientific supplied the SYBR Green/ROX qPCR Master Mix for qRT-PCR analysis. The primary antibodies against AKT, MMP2, MMP 9, BACL2, BAX, Cytochrome C, and the secondary antibodies used in this study were goat anti-rabbit immunoglobulin G (IgG) H & amp; L (HRP) (sc-2054), goat anti-mouse IgG-HRP (sc-2005) and mouse anti-rabbit IgG-HRP (sc-2357) were purchased from Santa Cruz Biotechnology (Dallas, TX, USA. All other substances and reagents used in this work were analytical grade and commercially accessible.

### 2.2. Cell lines and culture conditions

Four human cancer cell lines used in this study were as follows: MCF-7, MDA-MB-231, human breast adenocarcinoma, and MDA-MB-453 human triple-negative breast cancer cell lines were purchased from the American Type Culture Collection (ATCC) (Manassas, VA, USA). Two human lung normal cell lines L-132 (human embryonic pulmonary epithelial cell line) and MRC-5 (human fetal lung fibroblast cell line) were purchased from the Korean Cell Line Bank (Seoul, South Korea). MCF-7, MDA-MB-231, MDA-MB-453 cell lines were cultured with RPMI 1640 containing 10 % FBS and 1 % antibiotic-antimycotic solution under 5 % $CO_2$ at 37°C. Commercial standard drugs such as cisplatin, fluorouracil, and Doxorubicin were purchased from Sigma-Aldrich (St.

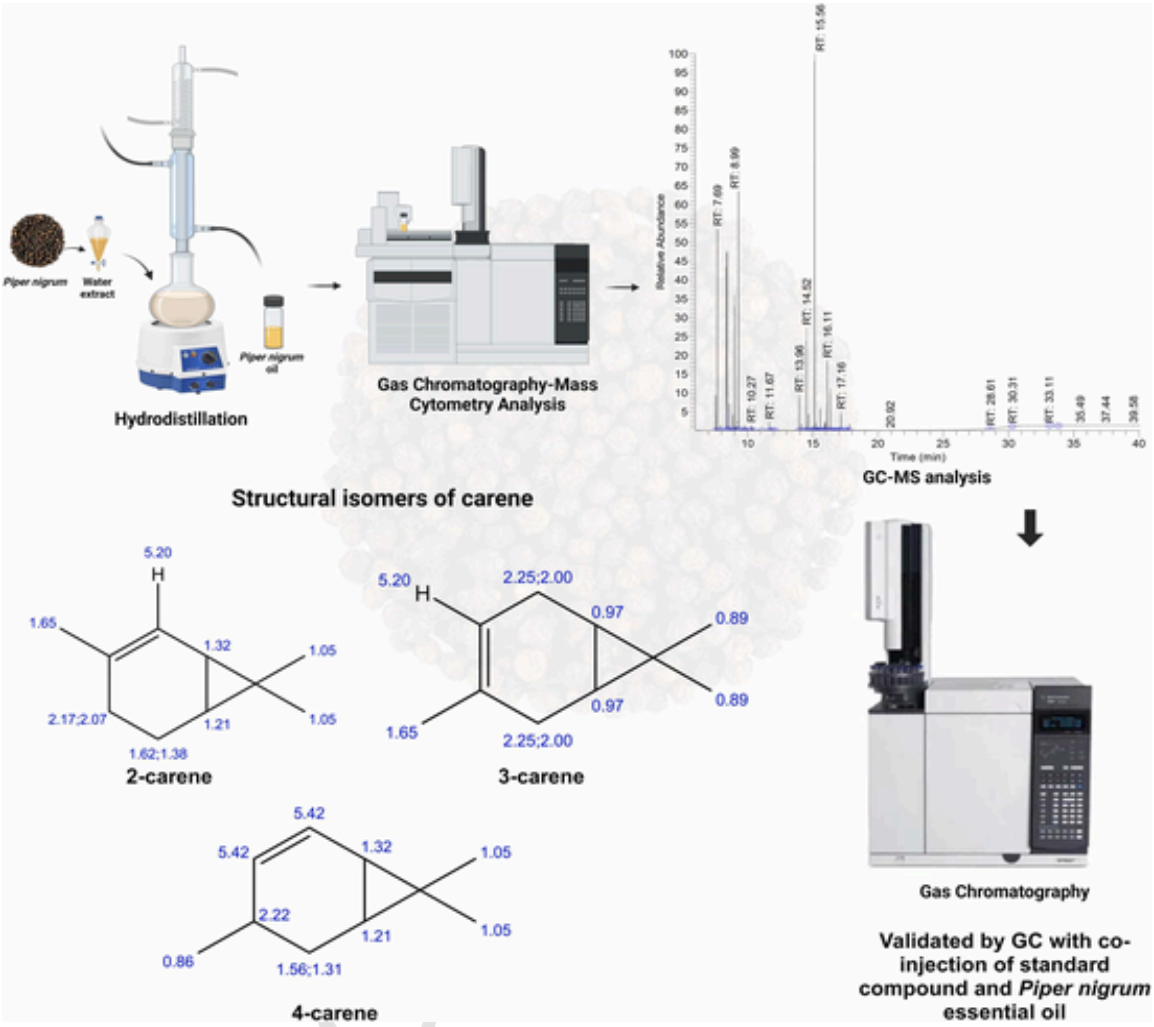


**Fig. 1.** Structures of 2-(1), 3-(2), and 4-carene (3). All three are isomers of carene with the same molecular formula ($C_{10}H_{16}$). Each contains a bicyclic structure with a cyclohexene ring and a cyclopropane ring and belongs to the class of bicyclic monoterpenes. The primary difference lies in the position of the double bond within the cyclohexene ring, which can affect their chemical reactivity and physical properties.

Louis, MO, USA). All chemicals used in this study were of a reagent-grade quality that was purchased commercially.

### 2.3. Steam distillation process

*Piper nigrum* dried seed (500 g) that had been air-dried was ground up and put through a two-hour steam distillation process at 100°C using a Clevenger-style apparatus. After being dried over anhydrous sodium sulfate, the volatile oil was kept in a sealed vial at 4°C until it was needed. The total yield was about 3 mL.

### 2.4. Chromatographic analysis

Isolation and identification of the active principles from *Piper nigrum* seed essential oil (PNS-EO) and gas chromatography (GC) were used in a setup with an auto-injector and flame ionization detector (FID). The Agilent 30 m × 0.32 mm i.d. (df = 0.25 μm) HP-5 capillary column (J&W Scientific, Folsom, CA) was used to separate the constituents. Based on a previous study (Kim et al., 2017; Perumalsamy et al., 2014) the oven temperature was set at 50°C (5 min isothermal) and gradually increased to 280°C at a rate of 5 °C per minute, followed by 10 minutes of isothermal operation. The chemical constituents have been identified using co-elution of standard samples after co-injection.

For gas chromatography-mass spectrometry (GC-MS) analysis, the Clarus 680/680 T gas chromatograph-mass spectrometer (PerkinElmer, Fort Belvoir, VA) was used. Similar columns and conditions used for GC-MS analysis were previously reported (Kim et al., 2017; Perumalsamy et al., 2014). The sector mass analyzer was programmed to scan from 35 to 550 amu every 0.2 seconds. The chemical contents were determined by comparing each peak's mass spectra to those of legitimate samples from a mass spectrum library.31

### 2.5. Antiproliferative assay

The antiproliferative activity of 3-carene in the human breast cancer cell lines was evaluated using a MTT assay described previously by Patravale et al., (Patravale et al., 2012). Briefly, the cytotoxic effect of carene isoforms, each cell was plated at $5 \times 10^3$ cells per well in 100 μL of complete culture medium containing several different concentrations of the test materials in 96 well microplates. The samples were dissolved in DMSO Hybri-Max. The final concentration of DMSO Hybri-Max in all assays was 0.1 % or less. The culture plates were incubated for 2 days in a 37°C incubator with a humidified atmosphere of 5 % $CO_2$. The plates were then washed one time with 100 μL PBS. The cell viability of treated and untreated cells was studied using MTT assay according to a previously reported method (Patravale et al., 2012).

**Table 2**
Chemical composition of PNS-EO using GC-MS analysis.

| Peak number | Compound | RT[a] (min) | % area in GC[b]-FID | Identification | |
|---|---|---|---|---|---|
| | | | | CI[c] | MS[d] |
| 1 | α-Thujene | 7.55 | 1.71 | O[e] | O |
| 2 | α-Pinene* | 7.69 | 10.83 | O | O |
| 3 | Camphene | 7.96 | 0.30 | O | O |
| 4 | Sabinene* | 8.37 | 10.79 | O | O |
| 5 | β-Pinene* | 8.45 | 10.10 | O | O |
| 6 | β-Myrcene | 8.62 | 1.57 | O | O |
| 7 | α-Phellandrene | 8.89 | 0.93 | O | O |
| 8 | δ−3-Carene* | 8.99 | 7.69 | O | O |
| 9 | α-Terpinene | 9.10 | 0.23 | | |
| 10 | Limonene* | 9.30 | 15.83 | | |
| 11 | (*Z*)-β-Ocimene | 9.58 | 0.14 | O | X[f] |
| 12 | γ-Terpinene | 9.79 | 0.30 | O | O |
| 13 | (*E*)-Sabinene hydrate | 9.94 | 0.10 | | |
| 14 | Terpinolene | 10.27 | 0.33 | | |
| 15 | Linalool | 10.39 | 0.23 | | |
| 16 | (*E*)-Pinocarveol | 11.12 | 0.03 | | |
| 17 | Terpinen−4-ol | 11.67 | 0.37 | | |
| 18 | α-Terpineol | 11.86 | 0.06 | | |
| 19 | Myrtenyl acetate | 12.09 | 0.02 | O | X |
| 20 | δ-Elemene | 13.96 | 1.41 | | |
| 21 | α-Cubebene | 14.13 | 0.27 | | |
| 22 | Cyclosativene | 14.43 | 0.11 | O | O |
| 23 | α-Copaene* | 14.52 | 4.13 | O | X |
| 24 | Aromadendrene | 14.69 | 0.70 | O | X |
| 25 | α-Gurjunene | 14.99 | 0.26 | O | X |
| 26 | Humulene | 15.15 | 0.89 | | |
| 27 | γ-Muurolene | 15.23 | 0.32 | O | X |
| 28 | α-Guaiene | 15.30 | 0.06 | | |
| 29 | (*E*)-β-Farnesene | 15.39 | 0.14 | | |
| 30 | (*Z*)-Muurola−1,5-diene | 15.50 | 0.05 | | |
| 31 | β-Caryophyllene* | 15.56 | 21.43 | O | X |
| 32 | γ-Muurolene | 15.79 | 0.19 | | |
| 33 | Germacrene D | 15.89 | 0.27 | | |
| 34 | β-Selinene | 15.97 | 0.44 | | |
| 35 | β-Bisabolene* | 16.11 | 3.94 | | |
| 36 | δ-Cadinene | 16.34 | 1.84 | | |
| 37 | - | 16.48 | 0.12 | | |
| 38 | - | 16.62 | 0.02 | | |
| 39 | (*E*)-Nerolidol | 16.72 | 0.04 | | |
| 40 | Caryophyllene oxide | 16.78 | 0.06 | | |
| 41 | β-Elemene | 16.84 | 0.03 | | |
| 42 | Spathulenol | 17.06 | 0.09 | | |
| 43 | Caryophyllene oxide | 17.16 | 0.89 | | |
| 44 | Humulene epoxide II | 17.46 | 0.03 | | |
| 45 | Spathulenol | 17.62 | 0.13 | | |
| 46 | α-Muurolol | 17.80 | 0.39 | | |

[a] Retention time.
[b] Gas-liquid chromatography with flame ionization detection.
[c] Co-injection with authentic samples.
[d] Mass spectrometry.
[e] Identified by co-injection or mass spectrometry.
[f] Unidentified by co-injection or mass spectrometry.
* Major constituent (>3 %).

### 2.6. Light microscopic analysis

MCF-7 cells were seeded onto 6-well culture plates at a density of 5 × $10^3$ cells per well overnight. The cells were treated with or without 2-, 3-, and 4-carene (0, 4, 8, 16, 32, and 64 μg/mL) in 0.1 % DMSO for 48 h. Cisplatin served as a reference control which was similarly prepared. Negative controls consisted of the DMSO solution. Morphological observations were made with a Leica DMIL LED equipped with an Integrated 5.0 Mega-Pixel MC 170 HD camera (Wetzlar, Germany).

**Table 3**
Antiproliferative activity of PNS-EO and its bioactive compounds toward MCF-7 cells using a MTT assay.

| Materials | Concentration (μg/mL) | |
|---|---|---|
| | 25 | 50 |
| PNS-EO[b] | 97.6 ± 0.34b | 100a |
| 3-Carene | 100a | 100a |
| β-Pinene | 97.8 ± 0.31b | 99.1 ± 0.14a |
| α-Pinene | 94.2 ± 0.85c | 98.8 ± 0.16b |
| α-Phellandrene | 91.3 ± 1.28c | 93.6 ± 0.94c |
| Camphene | 74.6 ± 3.75d | 98.9 ± 0.15b |
| Humulene | 73.1 ± 3.98d | 96.2 ± 0.56c |
| Terpinolene | 71.5 ± 4.21d | 74.7 ± 3.73d |
| β-Caryophyllene | 68.4 ± 3.82d | 74.2 ± 3.82d |
| (*E*)- β-Farnesene | 60.2 ± 5.89e | 73.8 ± 3.87d |
| β-Bisabolene | 45.7 ± 4.21 f | 63.8 ± 5.35 f |
| β-Myrcene | 41.2 ± 6.70 f | 45.1 ± 6.13 g |
| γ-Terpinene | 33.9 ± 6.78 g | 67.8 ± 4.76 f |
| Limonene | 26.1 ± 5.41 h | 78.8 ± 0.16d |
| Caryophyllene oxide | 17.9 ± 3.89i | 67.5 ± 4.80 f |
| α-Copaene | 8.98 ± 6.78j | 24.3 ± 5.35 h |
| (*E*)- Nerolidol | 0.81 ± 8.12k | 30.1 ± 6.13 h |
| Terpinen−4-ol | 0 l | 12.4 ± 6.96i |
| α-Terpinene | 0 l | 9.26 ± 7.43i |
| Aromadendrene | 0 l | 0j |
| Linalool | 0 l | 0j |
| Myrtenyl acetate | 0 l | 0j |
| (*Z*)-β-Ocimene | 0 l | 0j |
| (*E*)-Pinocarveol | 0 l | 0j |
| Spathulenol | 0 l | 0j |
| Sabinene | 0 l | 0j |
| α-Terpineol | 0 l | 0j |

*Means followed by the same letter in the column are not significantly different (p = 0.05, Bonferroni method). Values represent the percentage of inhibition of cell proliferation.

**Table 4**
Anti-proliferative activity of carene isoforms compared with standard drug cisplatin.

| Cell lines | Cisplatin | | 2-Carene | | 3-Carene | | 4-Carene | |
|---|---|---|---|---|---|---|---|---|
| | $IC_{50}$, μg/mL (95 % CL) | Slope ± SE | $IC_{50}$, μg/mL (95 % CL) | Slope ± SE | $IC_{50}$, μg/mL (95 % CL) | Slope ± SE | $IC_{50}$, μg/mL (95 % CL) | Slope ± SE |
| **MCF−7** | 11.16 (10.24–12.14) | 1.9 ± 0.09 | 22.04 (20.20–24.17) | 1.8 ± 0.08 | 11.19 (10.35–12.09) | 2.2 ± 0.08 | 14.70 (13.72–15.74) | 2.6 ± 0.11 |
| **MDA-MB−231** | 12.89 (11.80–14.08) | 1.8 ± 0.09 | 56.59 (51.75–62.22) | 2.9 ± 0.20 | 14.91 (13.82–16.11) | 2.2 ± 0.08 | 14.90 (13.76–16.17) | 1.9 ± 0.08 |
| **MDA-MB−453** | 18.02 (16.55–19.57) | 2.1 ± 0.09 | 38.68 (35.45–42.28) | 1.1 ± 0.08 | 12.04 (11.16–13.01) | 2.1 ± 0.08 | 16.27 (15.06–17.60) | 2.1 ± 0.08 |
| **MCF−7–12A** | 15.34 (14.29–16.44) | 2.7 ± 0.13 | 34.18 (31.65–37.11) | 2.5 ± 0.14 | 45.87 (42.34–50.18) | 2.7 ± 0.16 | 45.48 (41.89–49.89) | 2.6 ± 0.15 |
| **L−132** | 38.87 (33.20–45.09) | 1.2 ± 0.11 | 99.40 (89.79–112.25) | 2.1 ± 0.14 | 107.95 (96.92–123.0) | 2.1 ± 0.14 | 106.02 (95.08–121.0) | 2.1 ± 0.14 |
| **MRC−5** | 27.48 (25.46–29.69) | 2.2 ± 0.10 | 61.76 (57.59–66.55) | 2.4 ± 0.13 | 65.18 (60.65–70.47) | 2.3 ± 0.13 | 63.31 (58.97–68.33) | 2.3 ± 0.13 |

CL denotes confidence limits

### 2.7. Colony formation assay

MCF-7 cells (5 × $10^3$) were seeded in a 6-well plate. After adherence for 24 h, cells were washed with 1x PBS and treated with or without 0, 4, 8, 16, 32, and 64 μg/mL of 3-carene for 3 days. Then the cells were

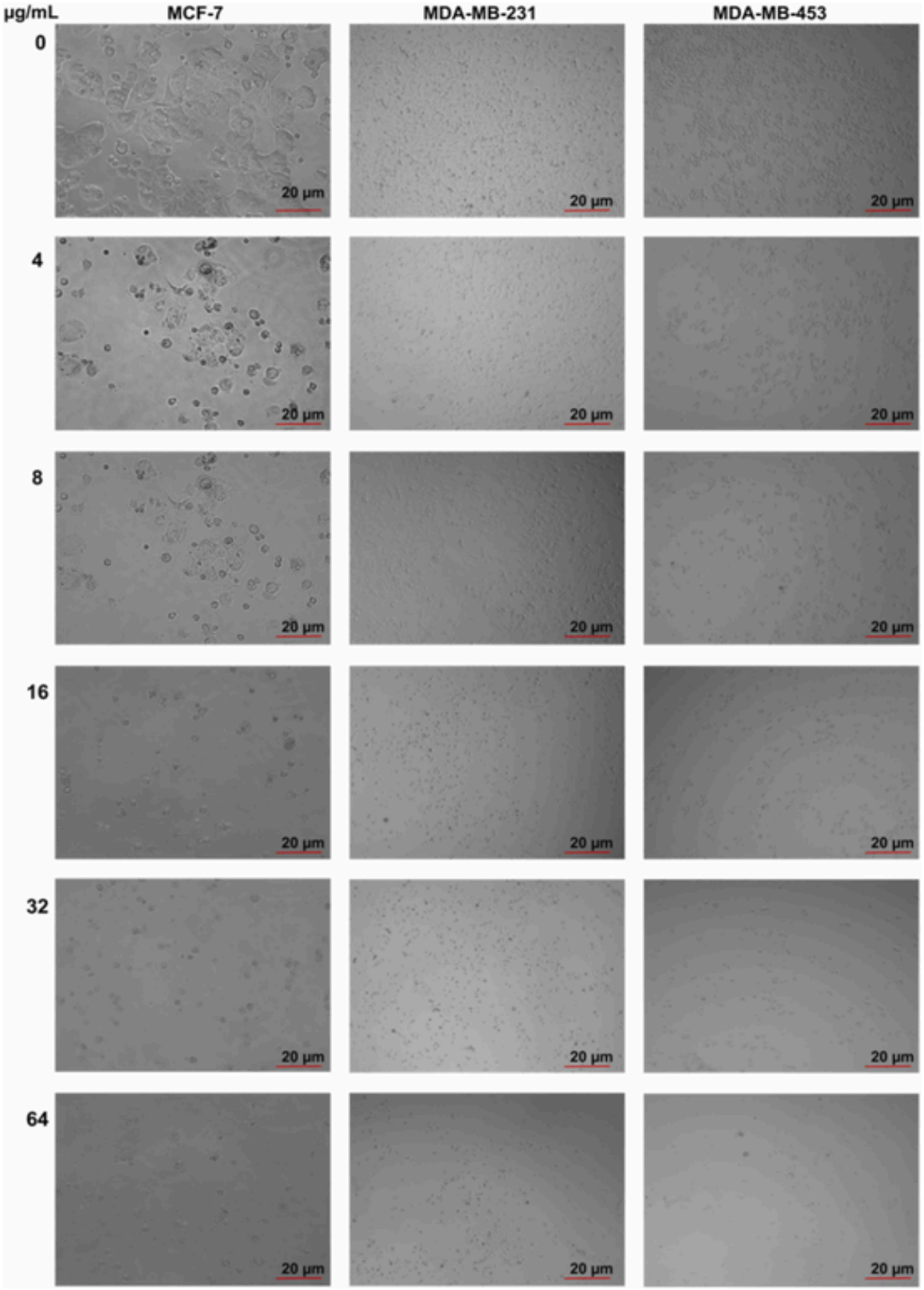


**Fig. 2.** Morphological changes of breast cancer cell lines (MCF-7) treated with 3-carene. MCF-7 cells (5 ×103/well) were treated with different concentrations of 3-carene for 48 h. Morphological observations were made with a phase contrast microscope (x20). Control cells exhibit typical morphology with normal features. Cells treated with varying concentrations of 3-carene demonstrate significant gradual morphological changes consistent with apoptosis, including cell shrinkage and membrane blebbing.

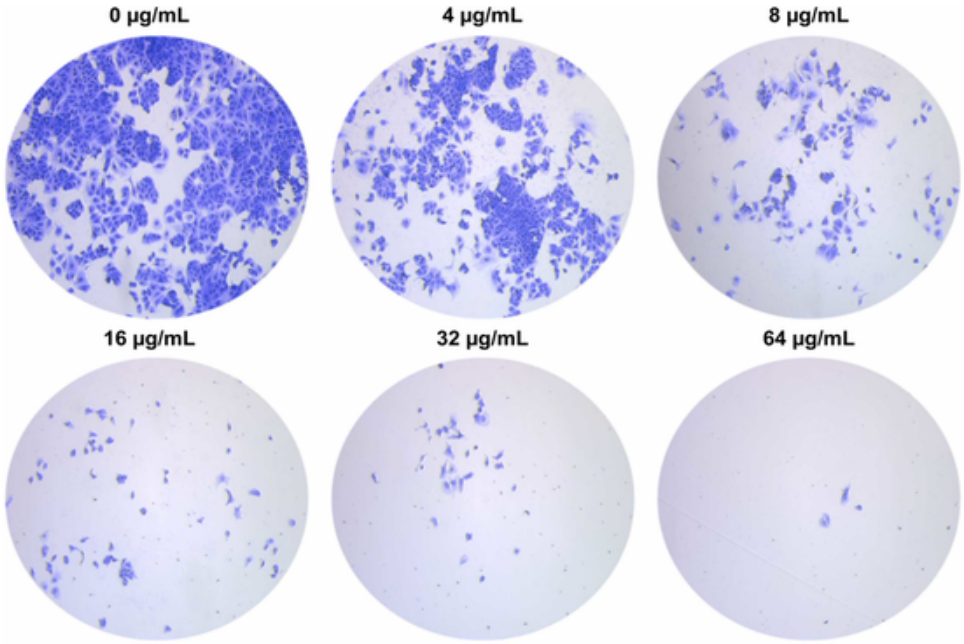


**Fig. 3.** Colony formation assay of 3-carene. 5 × 103/well MCF –7 cells treated with different concentrations of 3-carene and stained with crystal blue violet inhibited cell proliferation in a dose-dependent manner. The cells were visualized using light microscopy.

washed with 1x PBS, stained with trypan blue solution (Thermo Fisher Scientific, Waltham, MA, USA) for 5 min, and stained colonies were observed in an optimal light microscopy.

### *2.8. TUNEL assay*

MCF-7 cells were seeded at a density of 5 × $10^3$ cells/mL in 6-well plates with a glass coverslip. After a day of seeding, cells were treated with or without 3-carene for 4 days. Cells were washed and the culture medium was replaced on alternative days. At the end of the treatment, cells in coverslips were stained with 4 % paraformaldehyde/0.1 M PBS (pH 7–7.6) at room temperature for 30 min, and then washed with 1x PBS for further analysis. Later, cells were stained with a TUNEL assay kit according to manufacturer instructions. A negative control, without the addition of TdT enzyme, was included in each experiment. Finally, the cells were slightly counterstained with hematoxylin and visualized using light microscopy. Dark brown DAB signals indicated positive stained cells and blue shades signified unreacted cells.

### *2.9. Apoptotic cell propidium iodide and Hoechst 33258 staining*

MCF-7 cells were seeded onto 6-well culture plates at a density of 2 × $10^5$ cells per well overnight. The cells were treated with 3-carene (16 and 32 µg/mL) in 0.1 % DMSO for 48 h. Cells were then washed with 500 µL phosphate-buffered saline (PBS) and fixed with 4 % paraformaldehyde for about 15 min. They washed then with 500 µL PBS and stained with 500 µL PI (5 µg/mL) solution (Nicoletti, 2006) or with 500 µL Hoechst 33258 (10 µg/mL) solution (Ghate, 2013) in PBS at room temperature for 10 min. Apoptotic cells were evaluated using a Leica DMLB fluorescence microscope (Wetzlar, Germany).

### *2.10. Cell cycle analysis*

Cellular DNA contents were determined using flow cytometry to estimate the proportion of human cancer cells in different phases of the cell cycle affected by 3-carene. MCF-7 cells (2 × $10^5$/well) were treated with 3-carene (16 and 32 µg/mL) in 0.1 % DMSO for 48 h. The untreated (control) and treated cells were harvested, washed once with cold PBS (pH 7.4), and fixed in 70 % chilled ethanol at 4°C overnight. Cells were then centrifuged (300 × g for 5 min) and the pellet was resuspended in PBS containing 50 µg/mL PI and 100 µg/mL RNase A in darkness. Cell cycle analysis was performed using a FACS Calibur flow cytometer equipped with 488 nm (blue), 405 nm (violet), and 640 nm (red) solid-state laser light (BD Biosciences, San Jose, CA, USA). The percentage of cells in the different cell cycle phases was determined using the BD Biosciences Cell Quest acquisition software.

### *2.11. Annexin V/PI staining assay*

This assay was performed according to the protocol of the BD Pharmingen Annexin V-FITC Apoptosis Detection Kit (BD Biosciences). In brief, MCF-7 cells (2 × $10^5$/well) were treated with 0. 16, 32 µg/mL of 3-carene in 0.1 % DMSO for 2 days. Cells were harvested and washed twice with 500 µL cold PBS. After centrifugation (300 × g for 5 min), cells were suspended in 100 µL of binding buffer containing 5 µL annexin V-FITC and 5 µL PI staining solution. Cells were incubated at room temperature for 15 min in darkness. Finally, 400 µL of binding buffer was added before analysis on BD Biosciences FACSAria II flow cytometer. The data were analyzed using BD Biosciences FACSDiva software.

### *2.12. Real-time reverse transcription-PCR analysis*

Real-time qRT-PCR with SYBR Green dye was performed to determine whether 3-carene affected the expression levels of target gene (Bax, Bcl-2, Akt1, MMP-2, or MMP-9) mRNAs in MCF-7 cell lines. In brief, cultures of MCF-7 monolayers grown in 25 $cm^2$ cell culture flasks (Corning, NY, USA) were treated with 8, 16, and 32 µg/mL of 3-carene or cisplatin. After incubation at 37°C and 5 % $CO_2$ for 2 days, the total RNA was extracted from the non-treated and treated cultures using the RNeasy Mini Kit (Qiagen, Hilden, Germany) following the manufacturer's instructions. The residual genomic DNA was removed using RQ1 RNase-Free DNase (Promega, Madison, WI, USA). Complementary DNA (cDNA) was synthesized using 1 µg total RNA through a reverse tran-

**Table 5**
3-carene interaction with various receptors involved in regulation of cell cycle, and apoptosis.

| Receptor | PDB ID | Dock Score (Kcal/mol) | RMSD (Å) LB | RMSD (Å) UB | Interacting Residues |
|---|---|---|---|---|---|
| **CDK4** | 7SJ3 | −7.0 | 1.350 | 2.158 | VAL20, ALA33, VAL72, VAL96, LEU147, ALA157 |
| **PIK3CA** | 7L1B | −6.6 | 1.193 | 2.123 | PRO168, ARG662, TYR698, LEU752, PRO757, ALA758 |
| **CDK6** | 6OQO | −6.3 | 2.016 | 3.540 | TYR24, VAL27, ALA41, LEU152, ALA162, VAL77, PHE98 |
| **BCL-XL** | 3SPF | −6.2 | 1.497 | 2.451 | PHE97, PHE105, LEU108, PHE146 |
| **AKT1** | 7NH5 | −6.0 | 1.213 | 2.326 | TRP80, LEU210, LEU264, VAL270, TYR272 |
| **PTEN** | 1D5R | −5.9 | 1.741 | 3.891 | PHE206, LYS327, LYS330, TYR336, PHE337 |
| **BAX** | 1F16 | −5.6 | 1.129 | 3.992 | PHE92, PHE93, TRP139, ASP142, PHE143, GLU146 |
| **RB1** | 1N4M | −5.6 | 0.990 | 2.180 | LEU518, ALA525, LEU561, LEU564, LYS524 |
| **BAK** | 7M5B | −5.5 | 1.026 | 2.108 | ASP, 90, GLN94, TYR136, ARG137, LEU140 |
| **BCL−2** | 6GL8 | −5.3 | 1.482 | 2.127 | ALA131, VAL134, TYR180, TRP176 |
| **CCNE1** | 1W98 | −5.3 | 1.287 | 3.953 | LEU90, VAL101, MET105, VAL237, VAL250 |
| **CCND1** | 2W96 | −5.2 | 1.690 | 3.139 | ARG87, LEU91 |
| **Caspase 9** | 1NW9 | −5.0 | 1.275 | 1.275 | PRO338 |
| **Caspase 8** | 3KJN | −4.7 | 2.191 | 2.191 | PHE399 |
| **Cyt−6** | 6DUJ | −4.6 | 1.353 | 4.162 | LYS13, PHE82, VAL83 |
| **CDKN2A** | 7OZT | −4.6 | 2.176 | 4.425 | LEU104, VAL115, LEU130, ARG131, ALA134, |
| **Caspase 3** | 3GJQ | −4.2 | 5.359 | 7.336 | LEU74 |

scription reaction, according to the protocol of the SuperScript First-Strand Synthesis Kit (Invitrogen, Carlsbad, CA, USA). Five log10-fold dilutions of cDNA for each RNA were performed to determine PCR efficiency (100 ng–10 pg per reaction). qRT-PCR was performed in 96-well plates using the StepOnePlus Real-Time PCR System (Applied Biosystems, Foster, CA, USA). Each reaction mixture consisted of 10 μL Maxima SYBR Green/ROX qPCR Master Mix (2 ×) (Thermo Scientific, Foster, CA, USA), 2 μL of forward and reverse primers (5 pmol each), 1 μL cDNA (8 ng), and 7 μL double distilled water (DW) in a final volume of 20 μL. Oligonucleotide PCR primer pairs are listed in Table 1and were purchased from Bioneer (Daejeon, South Korea). The PCR conditions were as follows: 50°C for 2 min, 95°C for 10 min, and then 50 cycles of 95°C for 15 s and either 60°C (β-actin, Bax, Bcl-2, Akt1, MMP-2, or MMP-9) for 30 s. mRNA expression level of target gene was normalized to mRNA expression level for the housekeeping gene β-actin and analyzed by the $2^{-\Delta\Delta CT}$ method using Applied Biosystems StepOne Software v2.1 and DataAssist Software.

### 2.13. Western blot analysis

Briefly, 2 × $10^4$ MCF-7 cells were plated and treated with 0, 16, 32 μg/mL of 3-carene for 24 h. The western blot assay was carried out according to previously described (Xu et al., 2021) for apoptosis, cell cycle pathway, and metastasis proteins.

### 2.14. Data analysis

$IC_{50}$ value calculation, GraphPad Prism 5 (GraphPad Software, La Jolla, CA) was used. Furthermore, the SAS 9.13 software (SAS Institute, Cary, NC) was used to perform statistical analyses. A Student's *t*-test was used to evaluate the data from two groups, and a one-way analysis of variance and Bonferroni multiple comparison post-test were used to assess the data from different groups.

## 3. Results and discussion

### 3.1. Identification, and anti-cancer activity of bioactive components from PNS-EO

The 500 g of *Piper nigrum* seeds were hydro-distilled to produce pure PNS-EO oil while retaining highly volatile components. This hydro-distillation process was utilized to extract the entire active substance without losing components (Fig. 1). The active principles from PNS-EO were identified by GC-MS and the naming of each active constituent was confirmed by library search based on molecular formula and molecular weight closely matched (Table 2; Fig. 1). Based on the GC-MS analysis, we have identified more than 46 active constituents from PNS-EO. Among them, more than 8 were considered as major constituents based on % of the area (>3 %) detected by FID which includes, α-Pinene (10.83), Sabinene (10.79), β-Pinene (101.10), δ-3-Carene (7.69), Limonene (15.83), α-Copaene (4.13), β-Caryophyllene (21.43), and β-Bisabolene (3.94) respectively (Table 2). Though we have identified more than 46 active principles from PNS-EO based on a library database, we need to validate and confirm their presence in PNS-EO. Therefore, we have performed co-injection of commercially available standards for each constituent with PNS-EO individually and confirmed their peak with the same retention time for both standards as well as PNS-EO. Likewise, we have validated more than 17 compounds by GC analysis and reported in Table 2. Most of the remaining unidentified compounds were minor constituents and had very little effect on different cancer cell lines.

### 3.2. 3- Carene exhibited anti-proliferative activity against various breast cancer cells

The antiproliferative effects of PNS-EO and its bioactive constituents (27) on breast cancer lines (MCF-7) were validated using two different concentrations (25, 50 μg/mL) (Table 3). Among these, 3-carene had the greatest influence (100 %) on breast cancer lines MCF-7 at the lowest concentration compared to the other constituents. Based on the results, we further compared structural isomers of carene on different cancer lines. Therefore, we used 2-carene, 3-carene, and 4-carene to assess the anti-proliferative effect on breast cancer cell lines (MCF-7, MDA-MB-231, and MDA-MB-453). Among the three carenes tested on several breast cancer cell lines, 3-carene had the greatest effect on all of them (Table 4). The $IC_{50}$ values of 3-carene for MCF-7, MDA-MB-231, and MDA-MB-453 are 11.19 μg/mL, 14.91 μg/mL, and 12.04 μg/mL respectively (Table 4). However, we chose MCF-7 for further study as it showed the best anti-proliferative effect among other cell lines. Further, cell toxicity was also tested on three different normal cell lines (MCF-7–12A, L-132, and MRC-5) to evaluate the cell toxic effect of 3-carene (Table 4). Our investigation showed that 3-carene isomers had a significantly lower harmful effect on MCF-7–12A, L-132, and MRC-5 with $IC_{50}$ values of 45.87 μg/mL, 107.95 μg/mL, and 65.18 μg/mL respectively. The morphological changes observed in various cancer cells such as MCF-7, MDA-MB-231, and MDA-MB-453 treated with different isoforms of carene were compared with the standard drug, cisplatin as depicted in Fig. 2. Among three different forms, 3-carene is significantly involved in the induction of cell death, cell shrinkage, and cell number reduction. The colony formation inhibition,

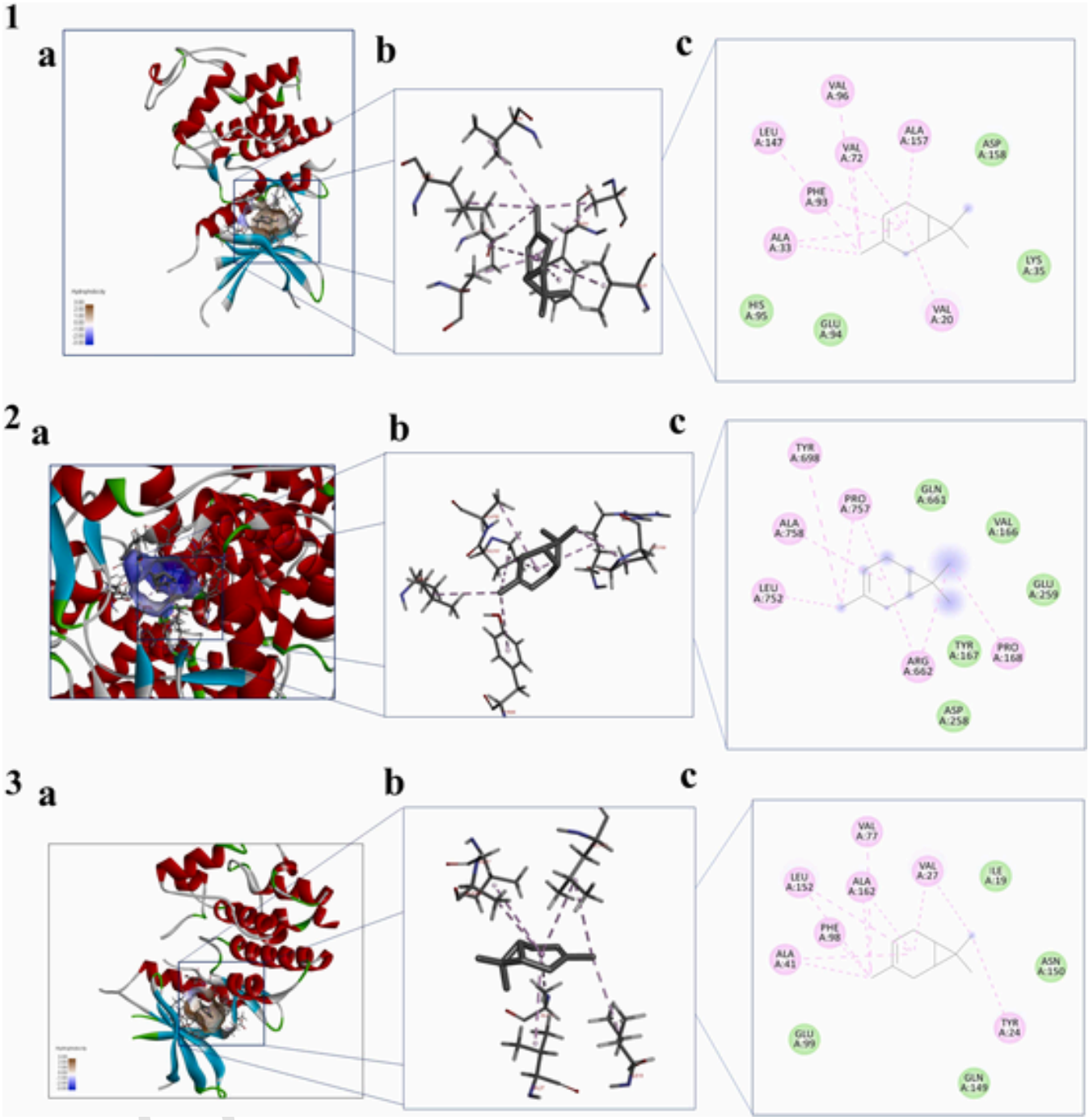


**Fig. 4.** 3-carene interacting with CDK4 (1), PIK3CA (2), and CDK6 (3). A. The 3D structure of the 3-carene molecular complex bound to target receptors. **B.** Display of interacting residues in a 3D orientation, highlighting critical points of interaction. **C.** Illustration of the binding site residues in a 2D schematic for enhanced molecular visualization.

cell number reduction, and cell proliferation suppression were also observed (Fig. 3). Studies have shown that the above morphological changes are hallmarks of apoptosis induction (Ahmed et al., 2023; Rollando et al., 2023). Therefore, we have carried out further studies using 3-carene.

### *3.3. 3-carene inhibits cell proliferation by targeting the cell cycle pathway*

Firstly, docking analysis was used to predict the 3-carene role in the cell cycle pathway. The dock scores represent the overall binding energy suggesting the potential binding of the 3-carene ligand with selected receptors **(**Table 5**).** 3-carene compounds have the highest dock score with CDK4 (-7.0 Kcal/mol), followed by PIK3CA (-6.6 Kcal/mol) and CDK6 (-6.3 Kcal/mol). suggesting a strong binding affinity with this receptor. The receptors have shown dock scores lesser than −6.0 Kcal mol except for AKT1 (-6.0 Kcal/mol). Similarly, receptors that have shown significant binding energy with 3-carene are AKT1 (-6.0 Kcal/mol), PTEN (-5.9 Kcal/mol), and RB1 (-5.6 Kcal/mol). Other receptors viz., caspase 3,8, and 9 exhibited dock score −5.0 Kcal or higher, CCND1 and CCNE1 −5.2 and −5.3 Kcal/mol respectively (Figs.

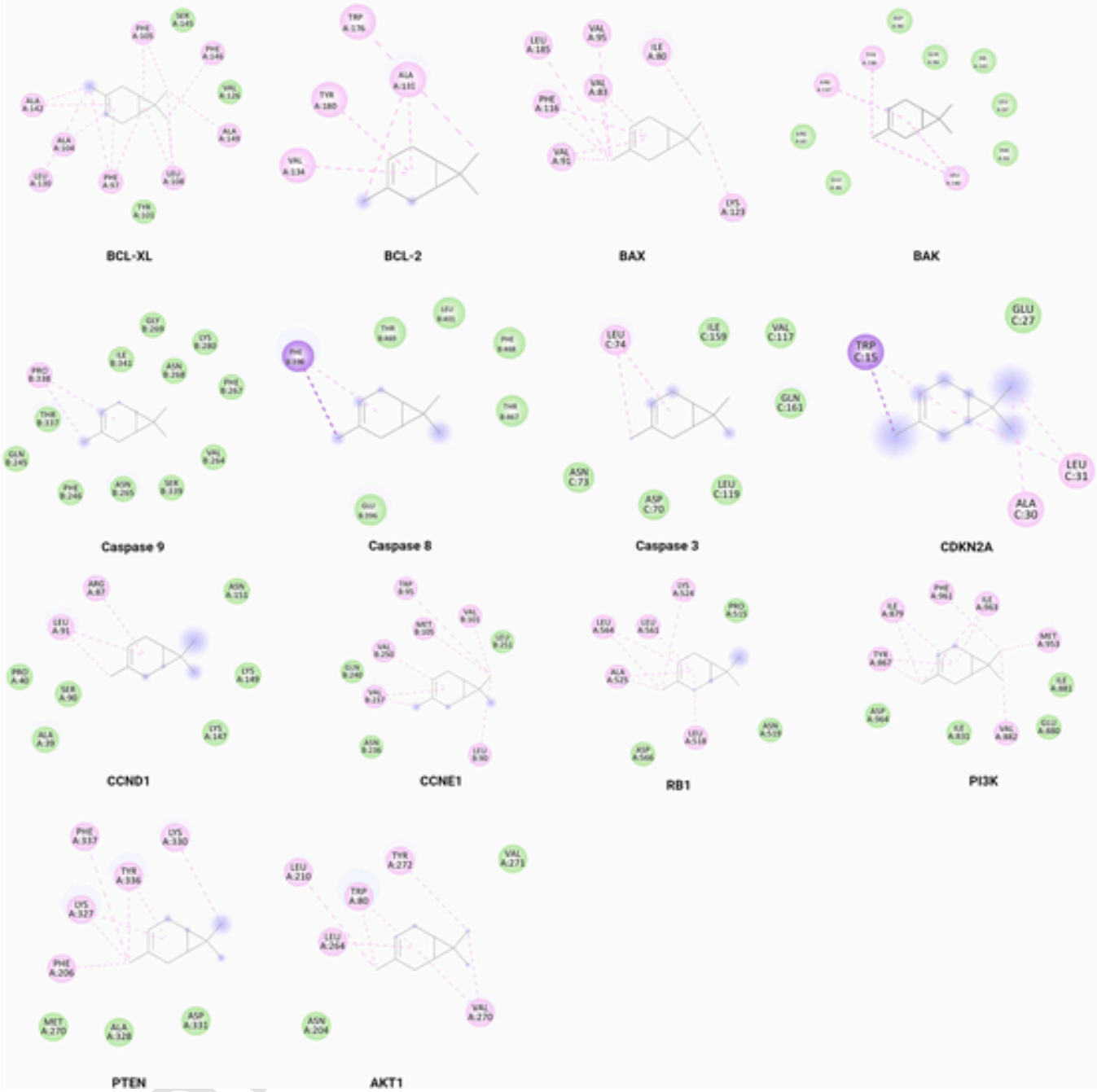


**Fig. 5.** 2D depiction of molecular interactions of 3-carene with selected cell cycle regulation and apoptosis regulator proteins obtained after molecular docking. This figure summarizes the key interaction points between 3-carene and proteins such as CDK4, PIK3CA, and CDK6, pivotal for cell cycle regulation and apoptosis, as derived from computational docking predictions.

4 & 5). The free binding energy (ΔG) estimated with Kdeep tool (https://open.playmolecule.org/tools/kdeep) for the specific docked poses of 3-carene with caspase 3,8, and 9 was estimated to be −3.5071, −3.3873 and −2.6728 kcal/mol. The corresponding estimated dissociation constant ($K_d$) were calculated to be 1.6 mM, 1.9 mM and 7.0 mM suggesting a moderate-to-weak binding affinity of 3-carene. This finding indicates that 3-carene exhibits a preferential interaction with Caspase 3, suggesting its potential role in modulating activity within the apoptotic signaling pathway. The slightly weaker binding affinity observed with Caspase 8 also implies a possible secondary role in the regulation of apoptosis, particularly within the extrinsic pathway. In contrast, the weak interaction with Caspase 9 suggests a minimal influence on the intrinsic apoptotic pathway. Such weak-to-moderate ΔG propose that 3-carene may function as an allosteric modulator, potentially altering Caspase 3 activity indirectly, rather than through direct inhibition or activation. The molecular interactions depicted in Fig. 5, between 3-carene and proteins such as CDK4, PIK3CA, and CDK6 are crucial for understanding the compound's potential anticancer effects. The observed decrease in Akt1 expression may indicate a suppression of cell survival signaling, as Akt is an important participant in supporting cell growth and survival. Cancer therapy targets the Akt pathway because of its function in cell survival (Simonyan et al., 2016). Akt expression

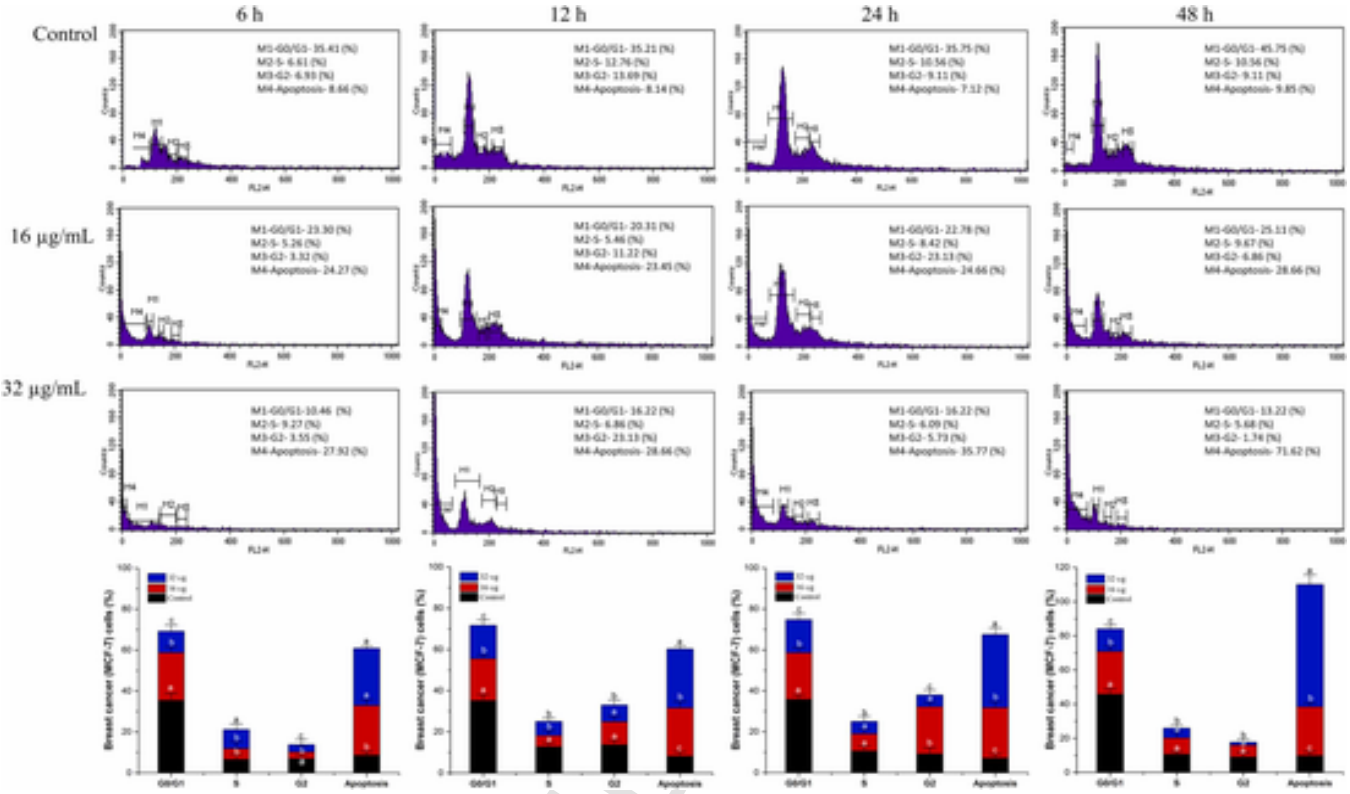


**Fig. 6.** Flow cytometric analysis of cell cycle progression and apoptotic cell death in 3-carene treated MCF-7 cells over time. A. Human breast cancer MCF-7 cells (2 ×105 cells/well) were treated with 32 µg/mL 3-carene for 6, 12, 24, and 48 h, while untreated cells served as controls. Post-treatment, cells were collected and fixed in 70 % cold ethanol at 4˚C overnight for cell cycle synchronization. Following fixation, cells were washed and then stained with a 50 µg/mL PI solution containing 100 µg/mL RNase to permit DNA content analysis. The flow cytometry procedure quantified both cell cycle distribution and apoptosis indicators. B. This bar graph summarizes the percentage of cell populations across different phases: G0/G1, S, and G2/M phases, as well as apoptotic cells in the sub-G1 phase. Data reflect the mean ± SE calculated from three independent experiments, underscoring the effect of 3-carene on cell cycle dynamics and its pro-apoptotic potential.

increases in a dose-dependent manner up to 16 µg/mL, indicating activation of cell survival pathways. However, the small decline in Akt phosphorylation at 32 µg/mL may indicate a cellular adaptive response to severe stress or a saturation point beyond which Akt no longer confers protective effects (Fadhal, 2023; Simonyan et al., 2016). These proteins are central to cell cycle regulation and apoptosis, and their modulation by 3-carene could lead to the inhibition of cancer cell proliferation and the induction of programmed cell death (Lim et al., 2019; Pfeffer and Singh, 2018; Singh et al., 2022). The 2D docking predictions suggest that 3-carene has a strong binding affinity to these proteins, which may disrupt their normal function. For instance, CDK4 and CDK6 are involved in the transition from the G1 phase to the S phase of the cell cycle, and their inhibition could result in cell cycle arrest (McCartney et al., 2019). Similarly, PIK3CA is part of the PI3K/AKT pathway, which promotes cell survival and proliferation, and its inhibition by 3-carene could lead to apoptosis (Xia et al., 2021). The induction of apoptosis is a key strategy in cancer therapy, and 3-carene's ability to bind to these proteins suggests it could trigger this process. The findings related to 3-carene can be compared to other studies where similar molecular interactions have been observed, such as aminoquinol, a CDK4/6 and PI3K/AKT inhibitor, which showed its potential efficacy in hepatocellular carcinoma. We confirmed docking results *in vitro* where 3-carene significantly arrested the cell cycle at S/G2 phase in a dose and time-dependent manner to induce apoptosis (Fig. 6). Specifically, 3-carene gradually induced cell cycle arrest in S/G2 phase at 6 h and peaked at 24 h, and then subsided. This shows that 3 carene causes apoptosis in a dose- and time-dependent way (Fig. 6). The bar graph of the figure shows that longer exposure to 3-carene causes a significant shift in the cell population to the sub-G1 phase, while the percentages of cells in the G0/G1, S, and G2/M phases decrease correspondingly. This shift is compatible with the activation of apoptosis, as cells with fragmented DNA, which is typical of late apoptotic stages, accumulate in the sub-G1 phase. The findings are consistent with the scientific literature, which shows that targeting the cell cycle and causing apoptosis are effective cancer therapies. For example, chemicals such as Valproic Acid have been demonstrated to cause cell cycle arrest in MCF-7 cells (Merelli et al., 2019). Similarly, Salidroside administration has been shown to alter the cell cycle and apoptosis in MCF-7 cells (Giordano et al., 2023). These findings lend support to the idea that regulating the cell cycle and apoptosis may be a potential treatment option for breast cancer. Furthermore, the larger ramifications of these findings are substantial. Because cell cycle dysregulation is a prevalent trait of cancer, 3-carene's capacity to induce cell cycle arrest may apply to various types of cancer cells. This calls for additional exploration into the methods by which 3-carene influences cell cycle checkpoints and the specific proteins implicated in cycle advancement.

### *3.4. 3-carene stimulated cell death by apoptosis induction*

Next, 3-carene induced apoptosis was confirmed both *in silico* and *in vivo*. For this, docking studies were first used to identify the interaction between important apoptosis signaling pathways and 3-carene. 3-Carene has shown relatively low RMSD values with BCL-XL, BCL-2, BAX, BAK, and PTEN, indicating that the docked poses are structurally more aligned and in proximity. However, some receptors have higher RMSD values (e.g., Caspase 3, CDKN2A, CCND1, and CCNE1). The

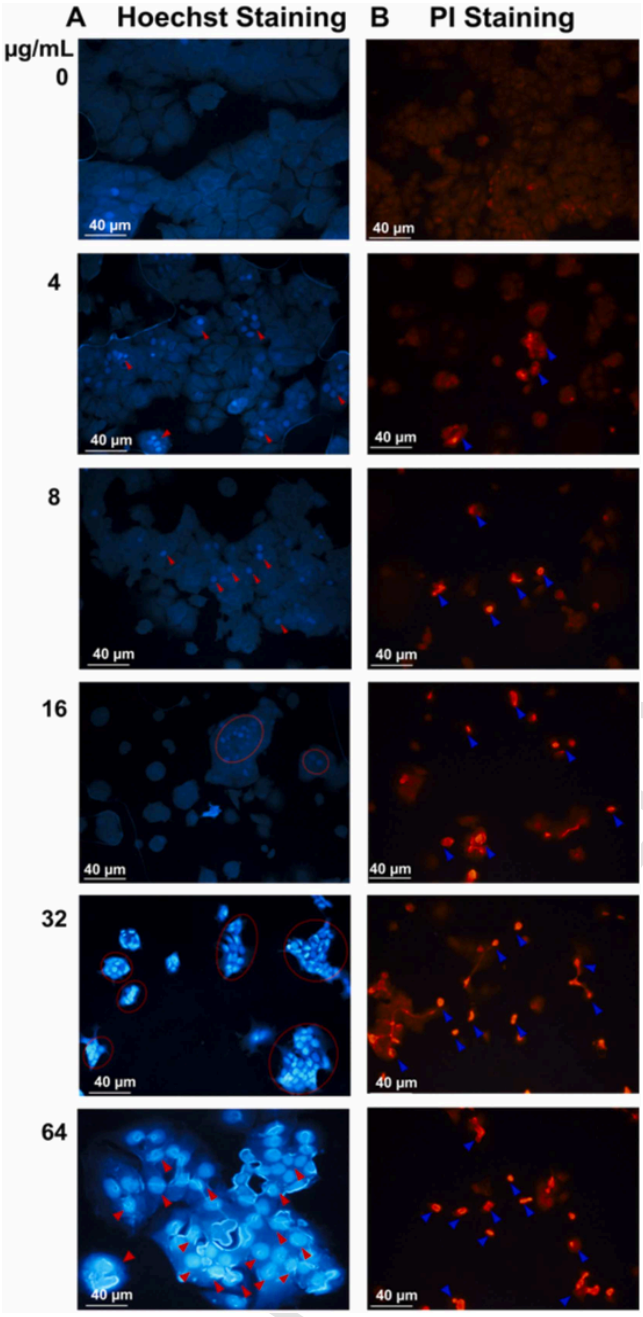


**Fig. 7.** Fluorescence micrographs of 3-carene treated MCF-7 cells stained with PI and Hoechst. MCF-7 cells ($2 \times 10^5$/well) were treated with 3-carene (16 and 32 µg/mL) for 48 h. Cells were washed with phosphate-buffered saline (PBS) and fixed with 4 % paraformaldehyde for about 15 min at room temperature. A & B. The cells were washed then with PBS and stained with 500 µL PI (5 µg/mL) or hoechst (10 µg/mL) solution in PBS at room temperature for 10 min. Apoptotic cells were evaluated using a fluorescence microscope (×20). Normal cells showed homogeneous staining of their nuclei. B. When MCF-7 cells were treated with different concentrations of 3-carene for 48 h, apoptotic cells showed irregular staining of their nuclei as a result of chromatin condensation and nuclear fragmentation. Normal cells showed homogeneous staining of their nuclei. The majority of 3-carene-treated AGS cells displayed a clear reduction in nuclear diameter and a complete derangement in chromatin structure. This morphological evaluation corroborates the apoptotic pathway activation induced by 3-carene treatment.

CDK4 which has exhibited highest dock score against 3-carene, interacts with VAL20, ALA33, VAL72, VAL96, LEU147, ALA157 of CD4. PIK3CA, the second receptor against which 3-carene has the second-highest dock score, interacts with PRO168, ARG662, TYR698, LEU752, PRO757, and ALA758. Against the CDK 6, 3-carene interacts with TYR24, VAL27, ALA41, LEU152, ALA162, VAL77, PHE98. With most of the receptors docked with 3-carene, it is noticeable that all the interactions are hydrophobic, however, they are either alkyl or Pi-alkyl. The key reason is that carene doesn't have any polar atoms which can contribute or receive any H-bonds. Accordingly, most interactions are reported with VAL and LEU. However, due to the bicyclic structure which may impart the partial negative charge within the cycles due to a double bond that results formation of Pi interactions often. 3-carene potentially interacts with CDK4, PIK3CA, and CDK6 (Fig. 4) which are key players in the complex regulation of cell cycle progression. Together with cyclin D, CDK4 forms a dynamic complex crucial for navigating the cell through the G1 phase and the decisive restriction point (Hindley and Philpott, 2013). This complex coordinates the phosphorylation of the retinoblastoma protein (Rb), liberating E2F transcription factors and triggering the expression of genes vital for DNA synthesis and cell cycle advancement (Ertosun et al., 2016). CDK4 also regulates the apoptotic pathway through interactions with the tumor suppressor protein p53. This interaction emphasizes the interplay between cell cycle regulation and the cellular decision between proliferation and apoptosis, highlighting the significance of CDK4 in maintaining cellular homeostasis (Stewart and Pietenpol, 2001). A study using delta-carene isolated from the essential oil of *Rosmarinus officinalis* L., *Cymbopogon citratus* (DC.) Stapf. has reported the cell cycle arrest in budding yeast (Kumar et al., 2021). Combinational treatment of 3-carene and artematrolide A have been found to demonstrate a significant cytotoxic activity on cervical cancer cells, by inducing G2/M cell cycle arrest and apoptosis by activating the ROS/ERK/mTOR signaling pathway and promoting the metabolic shift from aerobic glycolysis to mitochondrial respiration (Zhang et al., 2021). 3-carene which is a major constituent of *Pinus Roxburghii* essential oil suppressed the expression of NF-κB regulated gene products associated with cell survival (survivin, c-FLIP, Bcl-2, Bcl-xL, c-Myc, c-IAP2), proliferation (Cyclin D1), and metastasis (MMP-9). It also suppressed the activation of the inflammatory transcription factor NF-κB (Sajid et al., 2018). Fluorescence micrographs of MCF-7 cells treated with 3-carene and stained with propidium iodide (PI) and Hoechst 33258 (Fig. 7). These staining chemicals are widely employed in fluorescence microscopy to detect apoptotic cell changes (Jiang et al., 2009; Khanal et al., 2015). PI binds to DNA and is commonly used to detect late stages of apoptosis when membrane integrity is impaired, whereas Hoechst 33258 stains the nucleus and is effective for visualizing chromatin condensation and nuclear fragmentation (Khanal et al., 2015). The experiment shows that MCF-7 cells treated with 3-carene at doses of 4, 8, and 16 µg/mL gradually increased irregular nuclei patterns and peaked at 32, and 64 µg/mL respectively. These patterns show chromatin condensation and nuclear fragmentation, which are hallmarks of apoptosis (Khanal et al., 2015). The control cells had homogenous nuclear staining, indicating intact nuclei, but the treated cells had disordered nuclear morphology, defined by a reduction in nuclear diameter and disorganized chromatin structures (Khanal et al., 2015).

Fig. 8 suggests that 3-carene induces apoptosis in MCF-7 cells in a concentration-dependent manner. The increase in apoptotic cell populations and the decrease in viable cells indicate that 3-carene disrupts cellular homeostasis, leading to programmed cell death. The mechanism by which 3-carene triggers apoptosis could involve recognized apoptotic pathways, such as the internal mitochondrial pathway or the extrinsic death receptor system. Related investigations have demonstrated that chemicals like 3-carene can activate caspases and damage mitochondrial membranes, resulting in the release of cytochrome c and initiation of the apoptosis cascade (Kiraz et al., 2016; Shu et al., 2019).

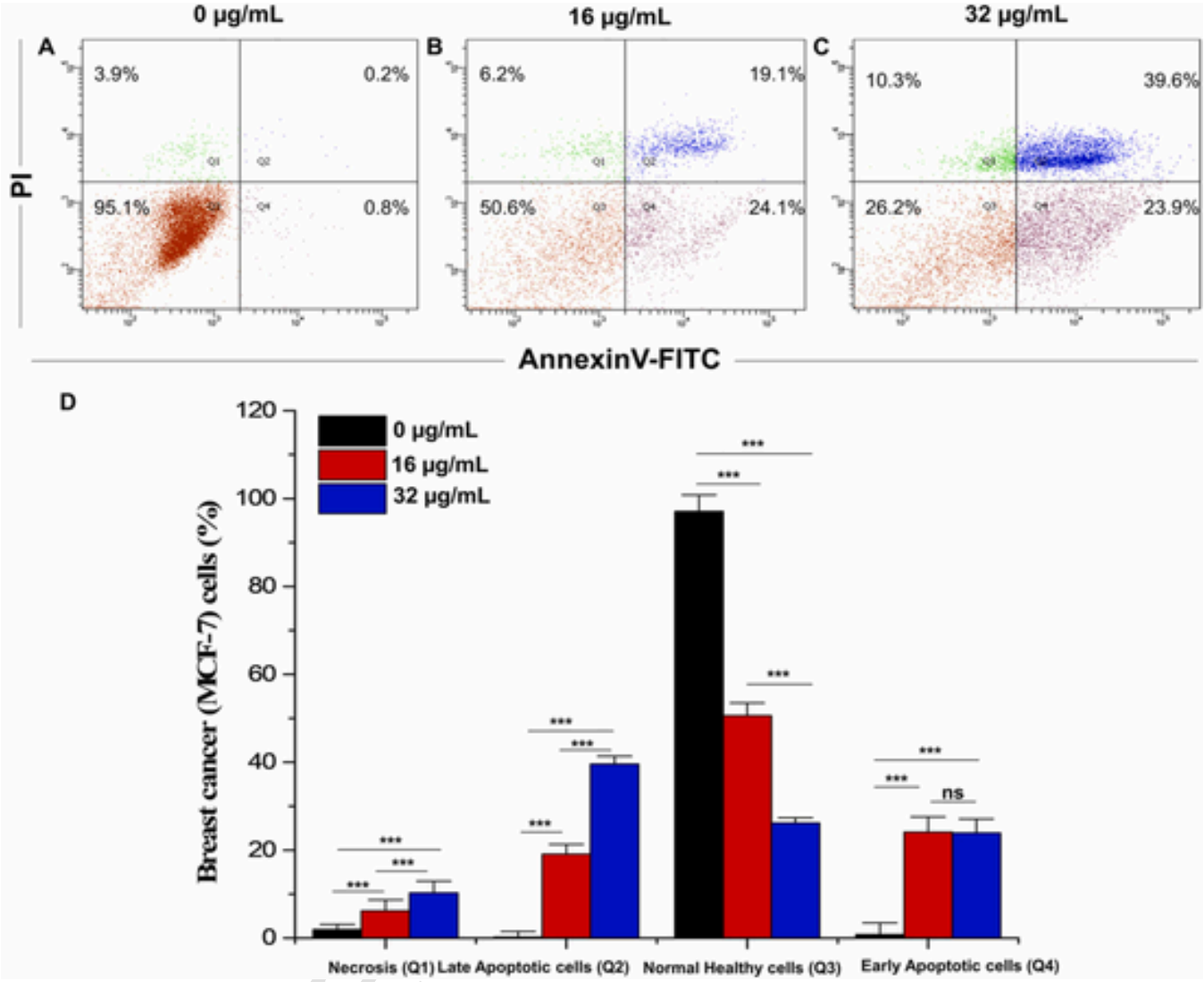


**Fig. 8.** Flow cytometric plots of Annexin V-FITC and PI staining of 3-carene treated MCF-7 cells. A. Human breast cancer MCF-7 cells ($2 \times 10^5$/well) were treated with different concentrations (0, 16, and 32 µg/mL) of 3-carene for 48 h. Cells were harvested and washed twice with cold phosphate-buffered saline (PBS, pH 7.4). After centrifugation (300 × g for 5 min), cells were suspended in 100 µL of binding buffer containing 5 µL of fluorescein isothiocyanate (FITC)-labeled Annexin V (Annexin V-FITC) (5 µg/mL) and 5 µL propidium iodide (PI) staining solution. Cells were incubated at room temperature for 15 min in darkness. Finally, 400 µL of binding buffer was added before analysis on a flow cytometer. B. Flow cytometric plots depict the concentration-dependent alteration in apoptosis induced by treatment with 16 and 32 µg/mL of 3-carene. The data illustrate a detailed analysis of the distribution of apoptotic stages: live cells (lower left quadrant, Q3), early apoptotic cells (lower right quadrant, Q4), late apoptotic cells (upper right quadrant, Q2), and necrotic cells (upper left quadrant, Q1). Data represent the mean ± SE of three experiments.

These findings emphasize the potential of 3-carene as a chemotherapeutic drug. However, more study, including *in vivo* investigations and clinical trials, is required to determine its efficacy and safety profile (Doostmohammadi et al., 2024; John et al., 2021). Comparing the performance of 3-carene to known chemotherapeutic drugs, such as doxorubicin, could shed light on its relative potency and potential advantages in terms of toxicity and side effects (Kashifa Fathima et al., 2022; Li et al., 2022). The apoptotic effects of 3-carene on MCF-7 cells offer valuable insights into its potential as an anticancer agent.

Further, 3-carene promotes apoptosis in a dose-dependent manner was confirmed using the TUNEL assay. Our result indicates DNA fragmentation associated with apoptosis as an increase in the number of apoptotic cells (green) was observed, as the concentration of 3-carene increases from 0 to 32 µg/mL (Fig. 9). This pattern is compatible with DAPI labeling, which labels all cell nuclei (blue), and the merged images indicate that apoptotic cells co-localize with the entire cell population. The dose-dependent effect of 3-carene on cell viability is an important finding. In the control group, the absence of green staining shows no apoptosis, however, when the concentration increases, green staining becomes increasingly visible, indicating that higher quantities of 3-carene are cytotoxic and cause cell death (Burgos Aceves et al., 2021; de Sousa et al., 2021). This phenomenon is consistent with the recognized concept of drug-induced apoptosis. As the quantity of a cytotoxic substance rises, so does the stress on cellular components, resulting in DNA damage and activation of apoptotic pathways. The TUNEL assay is a well-known approach for identifying such DNA fragmentation, and Fig. 9 results are consistent with earlier research that used this technique to investigate apoptosis (Mirzayans and Murray, 2020). Furthermore, DAPI labeling distinguishes between live and apoptotic cells, allowing for a more precise assessment of the apoptotic impact caused by 3-carene. This staining technique has been widely utilized in apoptosis

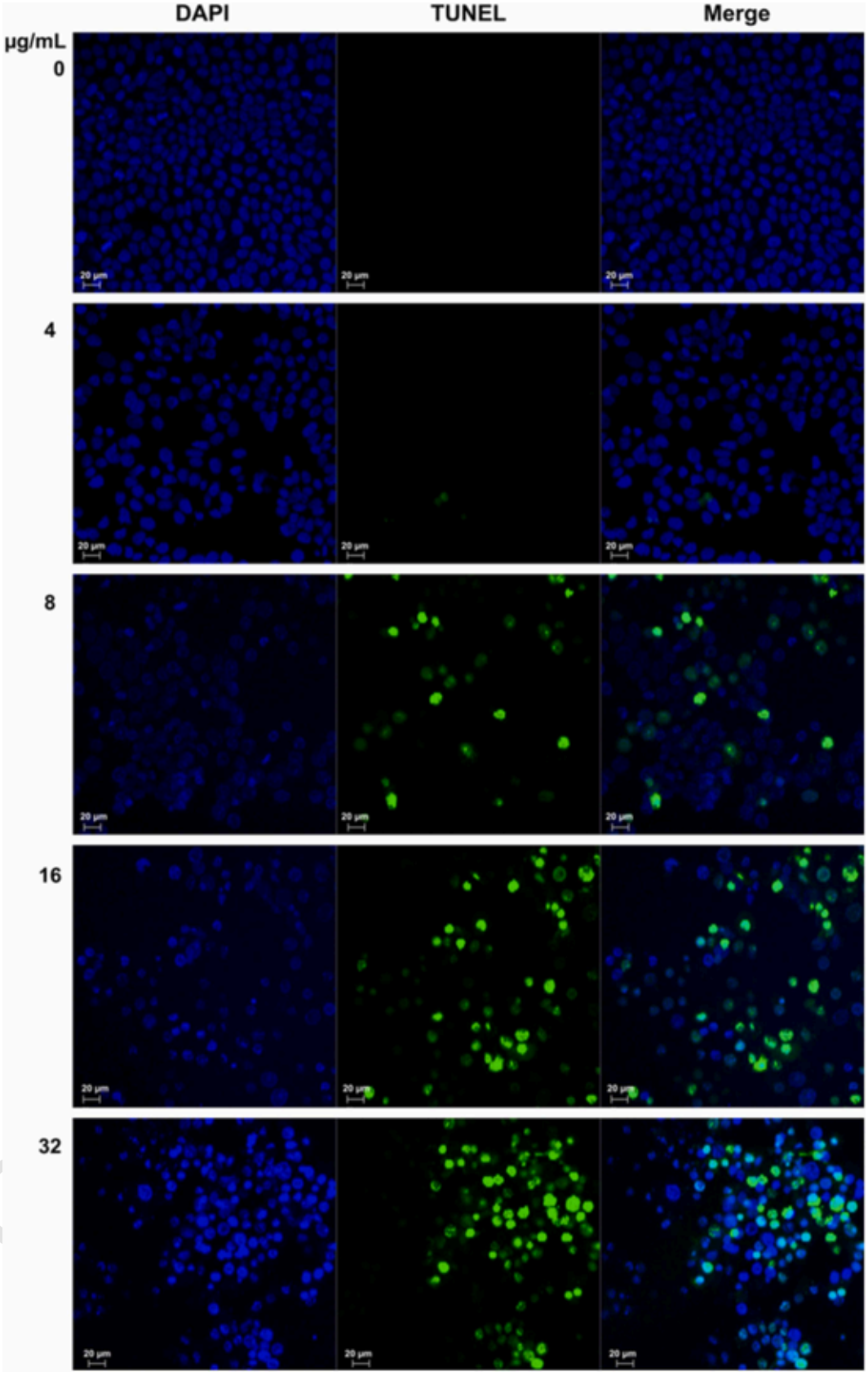
DAPI
TUNEL
Merge
μg/mL
0
4
8
16
32
20 μm

**Fig. 9.** TUNEL assay of cells treated with varying concentrations of 3-carene. Images show DAPI staining (blue) for total cell nuclei and TUNEL staining (green) for apoptotic cells at 0, 4, 8, 16, 32, and 64 μg/mL concentrations of 3-carene. The merged images highlight the co-localization of apoptotic cells within the total cell population. Scale bars represent 100 μM.

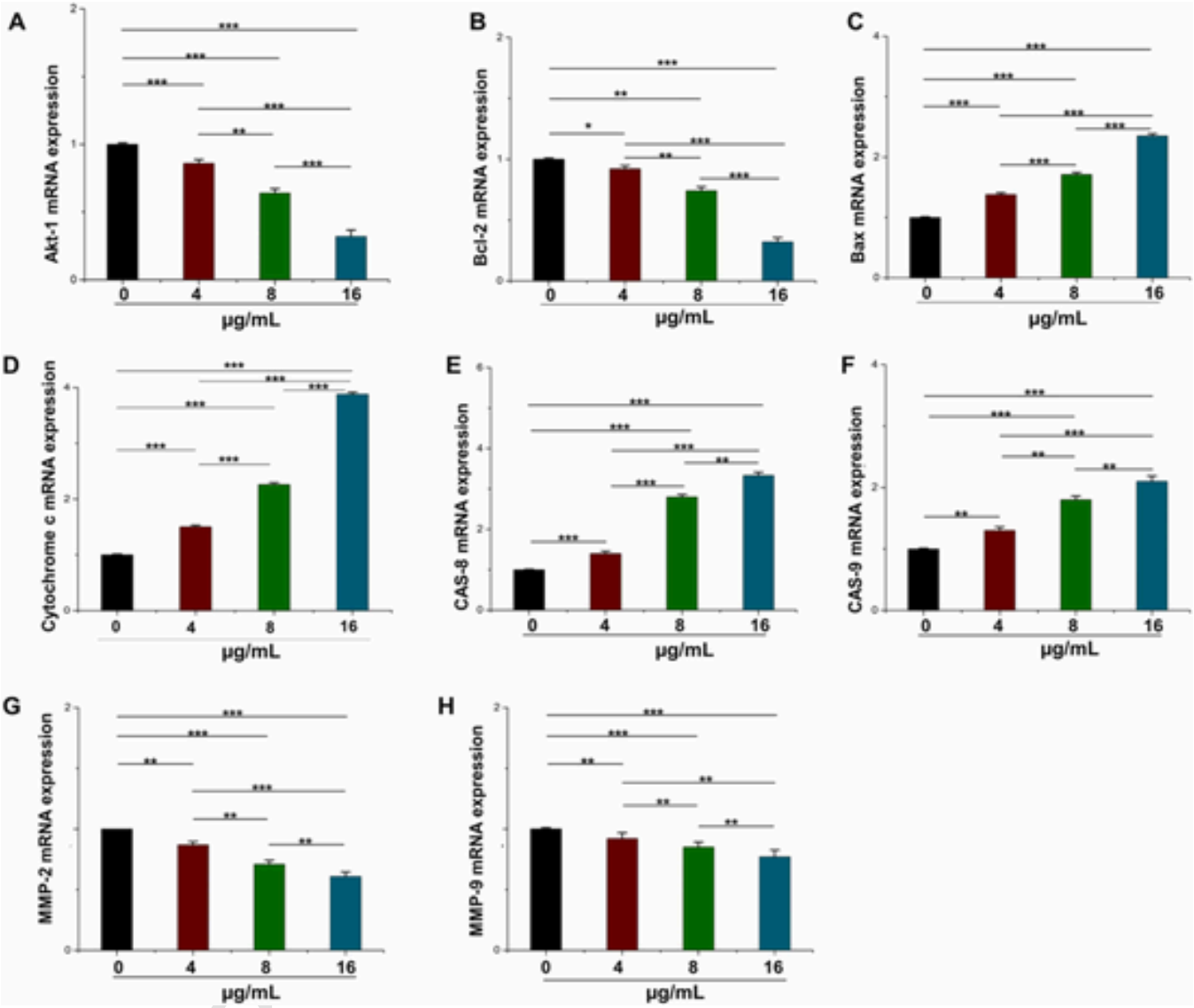


**Fig. 10.** Effect of 3-carene on the expression of the target gene mRNAs. Cultures of MCF-7 cells grown in cell culture flasks were treated with 4, 8, or 16 μg/mL 3-carene. After incubation at 37°C and 5 % $CO_2$ for 48 h, the total RNA was extracted from the non-treated and treated cultures. Real-time qRT-PCR was performed to determine the levels of *Bax*, *Bcl-2*, *Akt1*, *MMP-2*, and *MMP-9* mRNAs. Specific coding sequence primers were used to amplify the respective complementary DNAs, as described in the Methods section. Relative expression levels of mRNA of A. Bax, B. Bcl-2, C. Akt1, D. MMP-2, E. MMP-9. The mRNA expression was normalized to the constitutive expression of the mRNA for the housekeeping gene, β-actin, and analyzed by the $2^{-\Delta\Delta CT}$ method. Each bar represents the mean ± SE of duplicate samples run in three independent experiments ($^{***}P < 0.001$; $^{*}P < 0.05$; ns' no significant difference, using Bonferroni's multiple comparison test).

studies to detect changes in nuclear morphology and demonstrate the presence of programmed cell death (Mandelkow et al., 2017).

Additionally, Figs. 10 & 11 show that 3-carene has a dose-dependent effect on the expression of specific genes and proteins of MCF-7 cells using real-time PCR and western blot techniques. The findings indicate that increasing 3-carene concentrations causes an increase in Bax mRNA while decreasing Bcl-2, Akt1, MMP-2, and MMP-9 mRNA levels. This trend suggests that 3-carene may induce apoptosis while inhibiting cell survival and metastatic pathways. The rise in Bax expression and decrease in Bcl-2 expression are especially significant since they indicate a shift towards pro-apoptotic signaling within the cells. Bax is known to promote apoptosis, whereas Bcl-2 inhibits cell death. Furthermore, the drop in MMP-2 and MMP-9 suggests a possible decrease in the cells' ability to destroy the extracellular matrix, which is an important stage in cancer metastasis. These findings are consistent with the previous research on the roles of these genes in cancer. For example, regulating the Bax/Bcl-2 balance is a well-known approach in cancer therapy because it affects cancer cells' sensitivity to apoptosis (Alam et al., 2022; Salomons et al., 1999). The matrix metalloproteinases MMP-2 and MMP-9 are also important in cancer research since their activity is linked to tumor invasion and metastasis (Schroer et al., 2023). Furthermore, the antibacterial and probable anticancer qualities of 3-carene

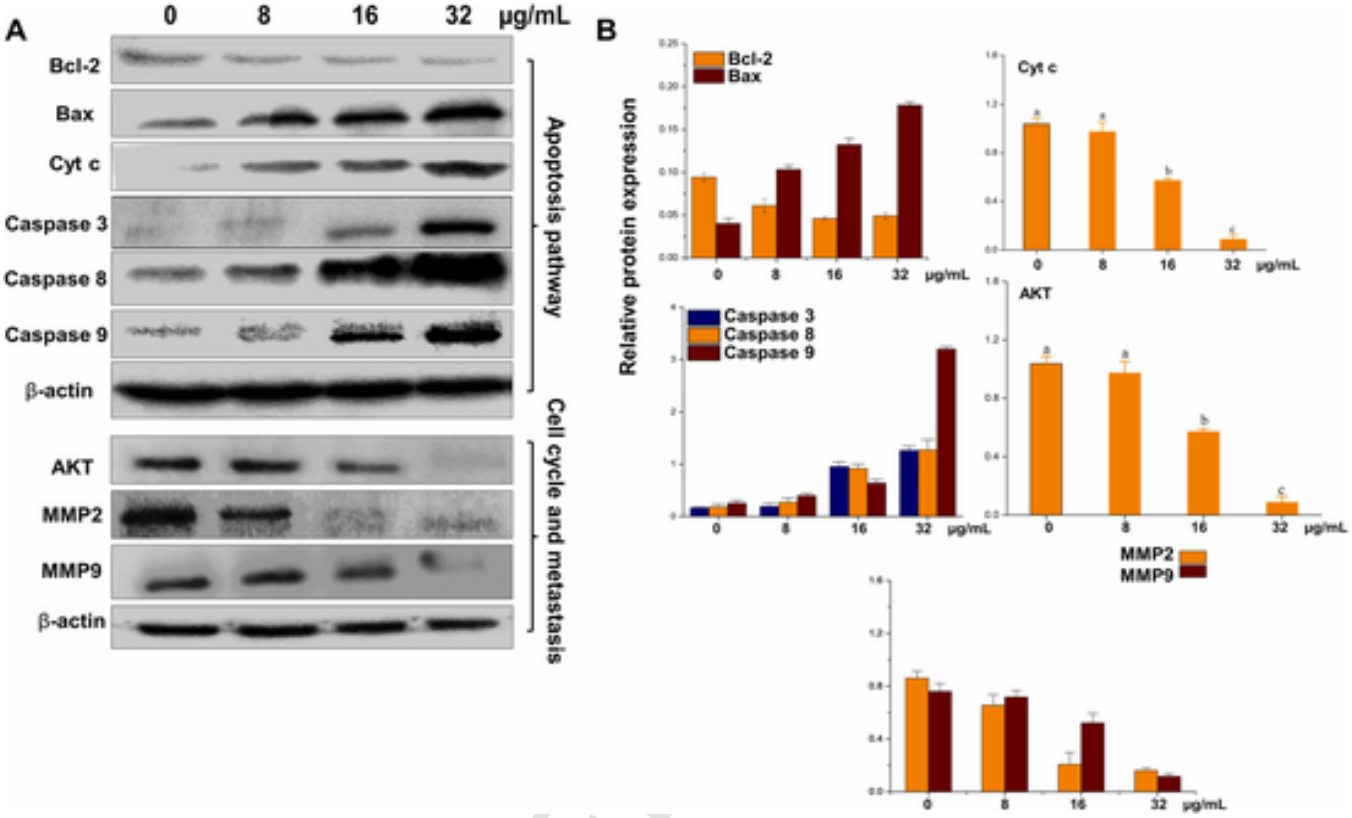


**Fig. 11.** Western blot analysis of protein expression in response to varying concentrations of 3-carene. The relative protein expression of Bax increases with concentration, suggesting enhanced pro-apoptotic signaling. Caspase-3 levels, showing significant increases at higher concentrations depicting apoptotic induction. Cytochrome c levels peaking at 32 µg/mL, implicating mitochondrial involvement in apoptosis. Bcl-2, anti-apoptotic that increasing could be a cellular attempt to counterbalance the apoptotic signals. Additionally, the relative protein expression of AKT, MMP2 and MMP9 was significantly decreased from the untreated breast cancer cells suggesting 3-carene role in cell cycle and apoptosis. B-actin served as a control and was used as normalized protein expression.

have been studied in scientific literature, implying that it might disrupt cell membranes and metabolic processes, thereby contributing to its pro-apoptotic effects. This is corroborated by research demonstrating that certain monoterpenes, particularly 3-carene, can induce apoptosis in cancer cells (Chaudhry et al., 2022; Shu et al., 2019). The interaction of pro-apoptotic proteins (Bax, Caspase-3, Cytochrome C) and anti-apoptotic signals (Akt, Bcl-2) demonstrates the complexities of apoptotic regulation. It shows that cells can respond to environmental stimuli in a finely calibrated manner, altering the balance between survival and death in order to maintain cellular integrity. Figs. 10 & 11 provides vital insights into the molecular basis of apoptosis and emphasizes the significance of dose-dependent effects in treatment efforts. Understanding these pathways is critical for developing therapeutics to successfully manage apoptosis in disorders characterized by dysregulated cell death. The findings also show the possibility of targeting individual components of the apoptotic process for therapeutic intervention.

## 4. Conclusion

Our combinational docking and *in vitro* analysis revealed that 3-carene from PNS-EO has the ability to target the cell cycle at S/G1 phase to activate the apoptosis pathway (Fig. 12). These findings suggest the use of 3-carene as a potential complementary drug and can be used in alternative medicine practice. Nevertheless, future studies on *in vivo* studies are warranted to explore their therapeutic potential against breast cancer.

## CRediT authorship contribution statement

**Saeedah Musaed Almutairi:** Formal analysis. **Sri Renukadevi Balusamy:** Writing – review & editing, Supervision, Methodology, Funding acquisition, Formal analysis. **Johan Sukweenadhi:** Methodology, Formal analysis. **Haribalan Perumalsamy:** Writing – original draft, Supervision, Methodology, Investigation. **Akhilesh Dubey:** Resources. **Anuj Ranjan:** Software. **Mohamed Farouk Elsadek:** Visualization. **Manohar Mahadev:** Validation. **Daewon Sohn:** Visualization, Validation.

## Declaration of Competing Interest

The authors declare no competing financial interests.

## Acknowledgements

This work was supported by Basic Science Research Program through the National Research Foundation of Korea (NRF) (Grant number 2020R1A6A1A06046728. The authors extend their appreciation to the Researchers Supporting Project number (RSP2024R418), King Saud University, Riyadh, Saudi Arabia.

## Data availability

No data was used for the research described in the article.

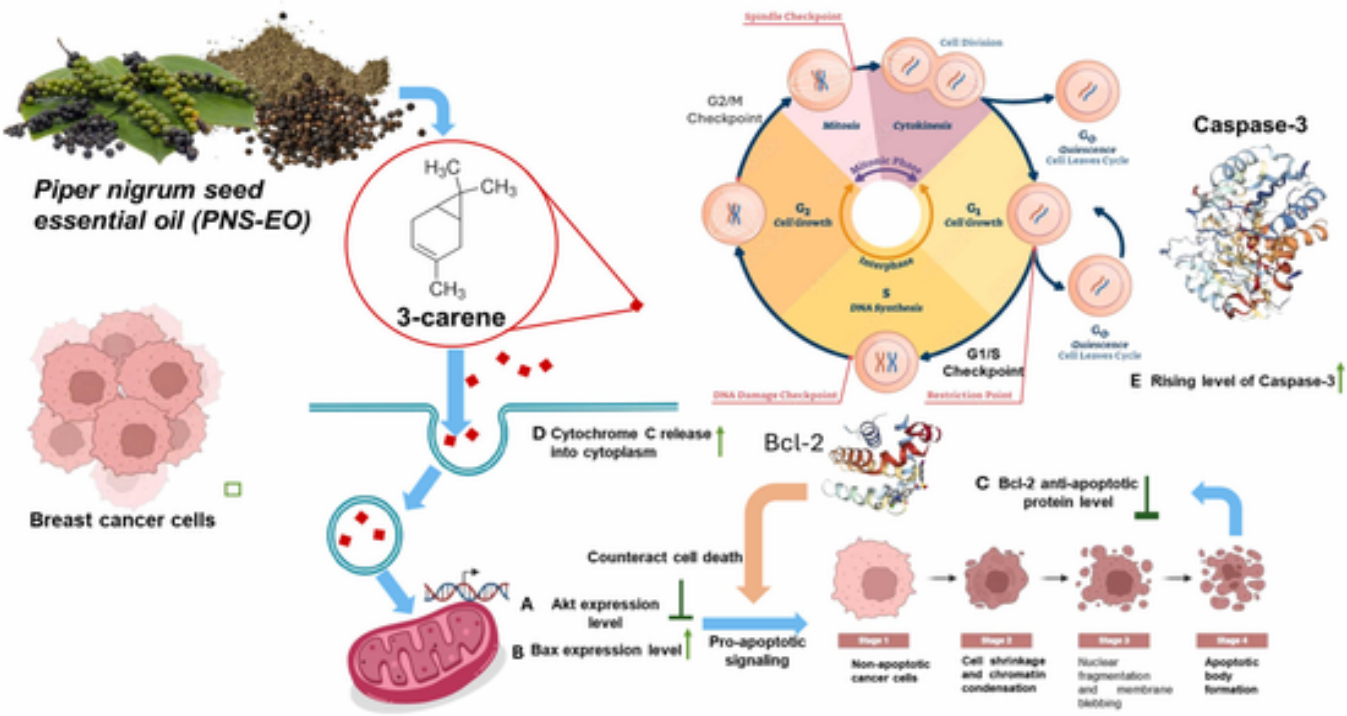


**Fig. 12.** Proposed mechanisms of 3-carene-induced G1/S and G2/M phase cell cycle arrest and apoptosis in MCF-7 cells.

## References


Ahmed, S.A., Al-Shanon, A.F., Al-Saffar, A.Z., Tawang, A., Al-Obaidi, J.R., 2023. Antiproliferative and cell cycle arrest potentials of 3-O-acetyl-11-keto-β-boswellic acid against MCF-7 cells in vitro. J. Genet. Eng. Biotechnol. 21, 75. https://doi.org/10.1186/s43141-023-00529-2.

Al-Khayri, J.M., Upadhya, V., Pai, S.R., Naik, P.M., Al-Mssallem, M.Q., Alessa, F.M., 2022. Comparative quantification of the phenolic compounds, piperine content, and total polyphenols along with the antioxidant activities in the Piper trichostachyon and P. nigrum. Molecules. https://doi.org/10.3390/molecules27185965.

Alam, M., Alam, S., Shamsi, A., Adnan, M., Elasbali, A.M., Al-Soud, W.A., Alreshidi, M., Hawsawi, Y.M., Tippana, A., Pasupuleti, V.R., Hassan, M.I., 2022. Bax/Bcl-2 Cascade Is Regulated by the EGFR Pathway: Therapeutic Targeting of Non-Small Cell Lung Cancer. Front. Oncol. 12. https://doi.org/10.3389/fonc.2022.869672.

Basholli-Salihu, M., Schuster, R., Hajdari, A., Mulla, D., Viernstein, H., Mustafa, B., Mueller, M., 2017. Phytochemical composition, anti-inflammatory activity and cytotoxic effects of essential oils from three Pinus spp. Pharm. Biol. 55, 1553–1560. https://doi.org/10.1080/13880209.2017.1309555.

Burgos Aceves, M.A., Migliaccio, V., Lepretti, M., Paolella, G., Di Gregorio, I., Penna, S., Faggio, C., Lionetti, L., 2021. Dose-Dependent Response to the Environmental Pollutant Dichlorodiphenileltylhene (DDE) in HepG2 Cells: Focus on Cell Viability and Mitochondrial Fusion/Fission Proteins. Toxics. https://doi.org/10.3390/toxics9110270.

Carneiro, B.A., El-Deiry, W.S., 2020. Targeting apoptosis in cancer therapy. Nat. Rev. Clin. Oncol. 17, 395–417. https://doi.org/10.1038/s41571-020-0341-y.

Chaudhry, G.-S., Md Akim, A., Sung, Y.Y., Sifzizul, T.M.T., 2022. Cancer and apoptosis: The apoptotic activity of plant and marine natural products and their potential as targeted cancer therapeutics. Front. Pharmacol. 13.

Clarke, S., 2008. In: Clarke, S.B.T.-E.C. for A. (Ed.), Chapter 7 - Composition of Essential Oils and Other Materials. Second E. (Ed., Churchill Livingstone, Edinburgh, pp. 123–229. https://doi.org/10.1016/B978-0-443-10403-9.00007-8.

de Sousa, I.F., Migliaccio, V., Lepretti, M., Paolella, G., Di Gregorio, I., Caputo, I., Ribeiro, E.B., Lionetti, L., 2021. Dose- and time-dependent effects of oleate on mitochondrial fusion/fission proteins and cell viability in HepG2 cells: comparison with palmitate effects. Int. J. Mol. Sci. https://doi.org/10.3390/ijms22189812.

Doostmohammadi, A., Jooya, H., Ghorbanian, K., Gohari, S., Dadashpour, M., 2024. Potentials and future perspectives of multi-target drugs in cancer treatment: the next generation anti-cancer agents. Cell Commun. Signal. 22, 228. https://doi.org/10.1186/s12964-024-01607-9.

Duan, Z., Xie, H., Yu, S., Wang, S., Yang, H., 2022. Piperine Derived from Piper nigrum L. Inhibits LPS-Induced Inflammatory through the MAPK and NF-κB Signalling Pathways in RAW264.7 Cells. Foods. https://doi.org/10.3390/foods11192990.

Ertosun, M.G., Hapil, F.Z., Osman Nidai, O., 2016. E2F1 transcription factor and its impact on growth factor and cytokine signaling. Cytokine Growth Factor Rev. 31, 17–25. https://doi.org/10.1016/j.cytogfr.2016.02.001.

Fadhal, E., 2023. A comprehensive analysis of the PI3K/AKT pathway: unveiling key proteins and therapeutic targets for cancer treatment. 11769351231194272. Cancer Inf. 22. https://doi.org/10.1177/11769351231194273.

Giordano, F., Paolì, A., Forastiero, M., Marsico, S., De Amicis, F., Marrelli, M., Naimo, G.D., Mauro, L., Panno, M.L., 2023. Valproic acid inhibits cell growth in both MCF-7 and MDA-MB231 cells by triggering different responses in a cell type-specific manner. J. Transl. Med. 21, 165. https://doi.org/10.1186/s12967-023-04015-8.

Hindley, C., Philpott, A., 2013. The cell cycle and pluripotency. Biochem. J. 451, 135–143. https://doi.org/10.1042/BJ20121627.

Jaidee, W., Maneerat, T., Rujanapun, N., Paojumroon, N., Duangyod, T., Banerjee, S., Kar, A., Mukherjee, P.K., Charoensup, R., 2022. Metabolite Fingerprinting of Piper nigrum L. from Different Regions of Thailand by UHPLC-QTOF-MS Approach and In Vitro Bioactivities. Trends Sci. 19, 1520. https://doi.org/10.48048/tis.2022.1520.

Jiang, M., Brooks, C., Dong, G., Li, X., Ni, H.-M., Yin, X.-M., Dong, Z., 2009. In: Dong, Z., Yin, X.-M. (Eds.), Analysis of Apoptosis: Basic Principles and Protocols BT - Essentials of Apoptosis: A Guide for Basic and Clinical Research. Humana Press, Totowa, NJ, pp. 691–711. https://doi.org/10.1007/978-1-60327-381-7_31.

John, P., Osani, M.C., Kodali, A., Buchsbaum, R., Bannuru, R.R., Erban, J.K., 2021. Comparative Effectiveness of Adjuvant Chemotherapy in Early-Stage Breast Cancer: A Network Meta-analysis. Clin. Breast Cancer 21, e22–e37. https://doi.org/10.1016/j.clbc.2020.07.005.

Kang, G.-Q., Duan, W.-G., Lin, G.-S., Yu, Y.-P., Wang, X.-Y., Lu, S.-Z., 2019. Synthesis of Bioactive Compounds from 3-Carene (II): Synthesis, Antifungal Activity and 3D-QSAR Study of (*Z*)- and (*E*)-3-Caren-5-One Oxime Sulfonates. Molecules. https://doi.org/10.3390/molecules24030477.

Kashifa Fathima, J., Lavanya, V., Jamal, S., Ahmed, N., 2022. The effectiveness of various chemotherapeutic agents in cancer treatment. Curr. Pharmacol. Rep. 8, 236–252. https://doi.org/10.1007/s40495-022-00289-6.

Khanal, G., Somaweera, H., Dong, M., Germain, T., Ansari, M., Pappas, D., 2015. In: Oslowski, C.M. (Ed.), Detection of Apoptosis Using Fluorescent Probes BT - Stress Responses: Methods and Protocols. Springer New York, New York, NY, pp. 151–161. https://doi.org/10.1007/978-1-4939-2522-3_11.

Kim, J.-R., Perumalsamy, H., Shin, H.M., Lee, S.-G., Ahn, Y.-J., 2017. Toxicity of Juniperus oxycedrus oil constituents and related compounds and the efficacy of oil spray formulations to Dermatophagoides farinae (Acari: Pyroglyphidae). Exp. Appl. Acarol. 73. https://doi.org/10.1007/s10493-017-0201-3.

Kiraz, Y., Adan, A., Kartal Yandim, M., Baran, Y., 2016. Major apoptotic mechanisms and genes involved in apoptosis. Tumor Biol. 37, 8471–8486. https://doi.org/10.1007/s13277-016-5035-9.

Kumar, A., Dev, K., Sourirajan, A., 2021. Essential Oils of Rosmarinus officinalis L., Cymbopogon citratus (DC.) Stapf., and the phyto-compounds, delta-carene and alpha-pinene mediate cell cycle arrest at G2/M transition in budding yeast Saccharomyces cerevisiae. South Afr. J. Bot. 141, 296–305. https://doi.org/10.1016/j.sajb.2021.05.008.

Li, B.-Y., Kang, G.-Q., Huang, Min, Duan, W.-G., Lin, G.-S., Huang, Mei, Wang, X., 2022. Synthesis, bioactivity and computational simulation study of novel (*Z*)-3-caren-5-one oxime ethers as potential antifungal agents. Res. Chem. Intermed. 48, 2135–2153.

https://doi.org/10.1007/s11164-022-04690-0.
Li, Y., Zhang, C., Pan, S., Chen, L., Liu, M., Yang, K., Zeng, X., Tian, J., 2020. Analysis of chemical components and biological activities of essential oils from black and white pepper (Piper nigrum L.) in five provinces of southern China. LWT 117, 108644. https://doi.org/10.1016/j.lwt.2019.108644.
Lim, B., Greer, Y., Lipkowitz, S., Takebe, N., 2019. Novel apoptosis-inducing agents for the treatment of cancer, a new arsenal in the toolbox. Cancers (Basel). https://doi.org/10.3390/cancers11081087.
Mandelkow, R., Gümbel, D., Ahrend, H., Kaul, A., Zimmermann, U., Burchardt, M., Stope, M.B., 2017. Detection and quantification of nuclear morphology changes in apoptotic cells by fluorescence microscopy and subsequent analysis of visualized fluorescent signals. Anticancer Res 37, 2239–2244. https://doi.org/10.21873/anticanres.11560.
McCartney, A., Migliaccio, I., Bonechi, M., Biagioni, C., Romagnoli, D., De Luca, F., Galardi, F., Risi, E., De Santo, I., Benelli, M., Malorni, L., Di Leo, A., 2019. Mechanisms of resistance to CDK4/6 inhibitors: potential implications and biomarkers for clinical practice. Front. Oncol. 9.
Merelli, A., Ramos, A.J., Lazarowski, A., Auzmendi, J., 2019. Convulsive Stress Mimics Brain Hypoxia and Promotes the P-Glycoprotein (P-gp) and Erythropoietin Receptor Overexpression. Recombinant Human Erythropoietin Effect on P-gp Activity. Front. Neurosci. 13.
Mirzayans, R., Murray, D., 2020. Do TUNEL and Other Apoptosis Assays Detect Cell Death in Preclinical Studies? Int. J. Mol. Sci. https://doi.org/10.3390/ijms21239090.
Patravale, V., Dandekar, P., Jain, R., 2012. 4 - Nanotoxicology: evaluating toxicity potential of drug-nanoparticles. In: Patravale, V., Dandekar, P., Jain, R.B.T.-N.D.D. (Eds.), Woodhead Publishing Series in Biomedicine. Woodhead Publishing, pp. 123–155. https://doi.org/10.1533/9781908818195.123.
Perumalsamy, H., Kim, J.Y., Kim, J.-R., Hwang, K.N.R., Ahn, Y.-J., 2014. Toxicity of basil oil constituents and related compounds and the efficacy of spray formulations to Dermatophagoides farinae (Acari: Pyroglyphidae). J. Med. Entomol. 51. https://doi.org/10.1603/ME13235.
Perumalsamy, H., Sankarapandian, K., Kandaswamy, N., Balusamy, S.R., Periyathambi, D., Raveendiran, N., 2017. Cellular effect of styrene substituted biscoumarin caused cellular apoptosis and cell cycle arrest in human breast cancer cells. Int. J. Biochem. Cell Biol. 92. https://doi.org/10.1016/j.biocel.2017.09.019.
Pfeffer, C.M., Singh, A.T.K., 2018. Apoptosis: A Target for Anticancer Therapy. Int. J. Mol. Sci. https://doi.org/10.3390/ijms19020448.
Rollando, R., Amelia, M.A., Afthoni, M.H., Prilianti, K.R., 2023. Potential Cytotoxic Activity of Methanol Extract, Ethyl Acetate, and n-Hexane Fraction from Clitoria ternatea L. on MCF-7 Breast Cancer Cell Line and Molecular Docking Study to P53. Ed. January-April 2023DO. J. Pure Appl. Chem. Res. 12 (1). https://doi.org/10.21776/ub.jpacr.2023.012.01.705.
Sajid, Arfaa, Manzoor, Q., Iqbal, M., Tyagi, A.K., Sarfraz, R.A., Sajid, Anam, 2018. Pinus Roxburghii essential oil anticancer activity and chemical composition evaluation. EXCLI J. 17, 233–245. https://doi.org/10.17179/excli2016-670.
Salomons, G.S., Smets, L.A., Verwijs-Janssen, M., Hart, A.A., Haarman, E.G., Kaspers, G.J., Wering, E.V., Der Does-Van Den Berg, A.V., Kamps, W.A., 1999. Bcl-2 family members in childhood acute lymphoblastic leukemia: relationships with features at presentation, in vitro and in vivo drug response and long-term clinical outcome. Leukemia 13, 1574–1580. https://doi.org/10.1038/sj.leu.2401529.
Schroer, J., Warm, D., De Rosa, F., Luhmann, H.J., Sinning, A., 2023. Activity-dependent regulation of the BAX/BCL-2 pathway protects cortical neurons from apoptotic death during early development. Cell. Mol. Life Sci. 80, 175. https://doi.org/10.1007/s00018-023-04824-6.
Sen, S., Gode, A., Ramanujam, S., Ravikanth, G., Aravind, N.A., 2016. Modeling the impact of climate change on wild Piper nigrum (Black Pepper) in Western Ghats, India using ecological niche models. J. Plant Res. 129, 1033–1040. https://doi.org/10.1007/s10265-016-0859-3.
Shu, H., Chen, H., Wang, X., Hu, Y., Yun, Y., Zhong, Q., Chen, Weijun, Chen, Wenxue, 2019. Antimicrobial Activity and Proposed Action Mechanism of 3-Carene against Brochothrix thermosphacta and Pseudomonas fluorescens. Molecules. https://doi.org/10.3390/molecules24183246.
Simonyan, L., Renault, T.T., da Costa Novais, M.J., Sousa, M.J., Côrte-Real, M., Camougrand, N., Gonzalez, C., Manon, S., 2016. Regulation of Bax/mitochondria interaction by AKT. FEBS Lett. 590, 13–21. https://doi.org/10.1002/1873-3468.12030.
Singh, V., Khurana, A., Navik, U., Allawadhi, P., Bharani, K.K., Weiskirchen, R., 2022. Apoptosis and Pharmacological Therapies for Targeting Thereof for Cancer Therapeutics. Sci. https://doi.org/10.3390/sci4020015.
Stewart, Z.A., Pietenpol, J.A., 2001. p53 Signaling and Cell Cycle Checkpoints. Chem. Res. Toxicol. 14, 243–263. https://doi.org/10.1021/tx000199t.
Takooree, H., Aumeeruddy, M.Z., Rengasamy, K.R.R., Venugopala, K.N., Jeewon, R., Zengin, G., Mahomoodally, M.F., 2019. A systematic review on black pepper (Piper nigrum L.): from folk uses to pharmacological applications. Crit. Rev. Food Sci. Nutr. 59, S210–S243. https://doi.org/10.1080/10408398.2019.1565489.
Turrini, E., Sestili, P., Fimognari, C., 2020. Overview of the Anticancer Potential of the "King of Spices" Piper nigrum and Its Main Constituent Piperine. Toxins (Basel). https://doi.org/10.3390/toxins12120747.
Woo, J., Yang, H., Yoon, M., Gadhe, C.G., Pae, A.N., Cho, S., Lee, C.J., 2019. 3-Carene, a Phytoncide from Pine Tree Has a Sleep-enhancing Effect by Targeting the $GABA_A$-benzodiazepine Receptors. Exp. Neurobiol. 28, 593–601. https://doi.org/10.5607/en.2019.28.5.593.
Xia, Z.-K., Wang, W., Qiu, J.-G., Shi, X.-N., Li, H.-J., Chen, R., Ke, K.-B., Dong, C., Zhu, Y., Wu, S.-G., Zhang, R.-P., Meng, Z.-R., Zhao, H., Gu, P., Leung, K.-S., Wong, M.-H., Liu, X.-D., Zhou, F.-M., Zhang, J.-Y., Yao, Y.-T., Wang, S.-J., Zhang, C.-Y., Qin, Y.-R., Lin, M.C., Jiang, B.-H., 2021. Discovery of a New CDK4/6 and PI3K/AKT Multiple Kinase Inhibitor Aminoquinol for the Treatment of Hepatocellular Carcinoma. Front. Pharmacol. 12.
Xu, X.Y., Tran, T.H.M., Perumalsamy, H., Sanjeevram, D., Kim, Y.-J., 2021. Biosynthetic gold nanoparticles of Hibiscus syriacus L. callus potentiates anti-inflammation efficacy via an autophagy-dependent mechanism. Mater. Sci. Eng. C. 124, 112035. https://doi.org/10.1016/j.msec.2021.112035.
Yu, L., Hu, X., Xu, R., Ba, Y., Chen, X., Wang, X., Cao, B., Wu, X., 2022. Amide alkaloids characterization and neuroprotective properties of Piper nigrum L.: A comparative study with fruits, pericarp, stalks and leaves. Food Chem. 368, 130832. https://doi.org/10.1016/j.foodchem.2021.130832.
Zhang, X.-T., Hu, J., Su, L.-H., Geng, C.-A., Chen, J.-J., 2021. Artematrolide A inhibited cervical cancer cell proliferation via ROS/ERK/mTOR pathway and metabolic shift. Phytomedicine 91, 153707. https://doi.org/10.1016/j.phymed.2021.153707.